

**ON THE PASSIVITY OF
INTERACTION CONTROL WITH
SERIES ELASTIC ACTUATION**

by

Fatih Emre Tosun

**Submitted to
the Graduate School of Engineering and Natural Sciences
in partial fulfillment of
the requirements for the degree of
Master of Science**

SABANCI UNIVERSITY

July 2019

© Fatih Emre Tosun 2019
All Rights Reserved

ON THE PASSIVITY OF
INTERACTION CONTROL WITH
SERIES ELASTIC ACTUATION

APPROVED BY

Assoc. Prof. Dr. Volkan Patoglu
(Thesis Advisor)



Prof. Dr. Çağatay Başdoğan



Assoc. Prof. Dr. Kemalettin Erbatur



DATE OF APPROVAL: 09.08.2019

ABSTRACT

ON THE PASSIVITY OF INTERACTION CONTROL WITH SERIES ELASTIC ACTUATION

Fatih Emre Tosun

Mechatronics Engineering, M.Sc. Thesis, July 2019

Thesis Advisor: Assoc. Prof. Dr. Volkan Patoglu

Keywords: Physical human-robot interaction, series elastic actuation, frequency domain passivity, coupled stability, impedance control, haptic rendering

Regulating the mechanical interaction between robot and environment is a fundamentally important problem in robotics. Many applications such as manipulation and assembly tasks necessitate interaction control. Applications in which the robots are expected to collaborate and share the workspace with humans also require interaction control. Therefore, interaction controllers are quintessential to physical human-robot interaction (pHRI) applications.

Passivity paradigm provides powerful design tools to ensure the safety of interaction. It relies on the idea that passive systems do not generate energy that can potentially destabilize the system. Thus, coupled stability is guaranteed if the controller and the environment are passive. Fortunately, passive environments constitute an extensive and useful set, including all combinations of linear or nonlinear masses, springs, and dampers. Moreover, a human operator may also be treated as a passive network element. Passivity paradigm is appealing for pHRI applications as it ensures stability robustness and provides ease-of-control design. However, passivity is a conservative framework which imposes stringent limits on control gains that deteriorate the performance. Therefore, it is of paramount importance to obtain the most relaxed passivity bounds for the control design problem.

Series Elastic Actuation (SEA) has become prevalent in pHRI applications as it provides considerable advantages over traditional stiff actuators in terms of stability robustness and fidelity of force control, thanks to deliberately introduced compliance between the actuator and the load. Several impedance control architectures have been proposed for SEA. Among the alternatives, the cascaded controller with an inner-most velocity loop, an intermediate torque loop and an outer-most impedance loop is particularly favoured for its simplicity, robustness, and performance.

In this thesis, we derive the necessary and sufficient conditions to ensure the passivity of the cascade-controller architecture for rendering two classical linear impedance models of null impedance and pure spring. Based on the newly established passivity conditions, we provide non-conservative design guidelines to haptically display free-space and virtual spring while ensuring coupled stability, thus the safety of interaction. We demonstrate the validity of these conditions through simulation studies as well as physical experiments.

We demonstrate the importance of including physical damping in the actuator model during derivation of passivity conditions, when integral controllers are utilized. We note the unintuitive adversary effect of actuator damping on system passivity. More precisely, we establish that the damping term imposes an extra bound on controller gains to preserve passivity.

We further study an extension to the cascaded SEA control architecture and discover that series elastic damping actuation (SEDA) can passively render impedances that are out of the range of SEA. In particular, we demonstrate that SEDA can passively render Voigt model and impedances higher than the physical spring-damper pair in SEDA. The mathematical analyses of SEDA are verified through simulations.

ÖZETÇE

Seri Elastik Eyleyicili Etkileşim Kontrolcülerinin Pasifliği

Fatih Emre Tosun

Mekatronik Mühendisliği, Yüksek Lisans Tezi, Temmuz 2019

Tez Danışmanı: Doç. Dr. Volkan Patoğlu

Anahtar Kelimeler: Fiziksel insan-robot etkileşimi, seri elastik eyleyici, frekans uzayında pasiflik, bileşke kararlılık, empedans kontrolü, haptik gerçekleştirme

Robot ve çevre arasındaki mekanik etkileşimi düzenlemek, robot biliminde önemli bir problemdir. Manipülasyon ve montaj işleri gibi birçok uygulama etkileşim kontrolcüsü gerektirir. Robotların insanlarla birlikte çalışması ve çalışma alanını paylaşması gereken uygulamalarda da etkileşim kontrolcüsü gereklidir. Bu nedenle etkileşim kontrolcüleri fiziksel insan-robot etkileşimi (fİRE) uygulamaları için fevkalade önemlidir.

Pasiflik paradigması etkileşimin güvenliğini sağlamak için güçlü tasarım araçları sunar. Bu paradigma pasif sistemlerin enerji üretme potansiyeline sahip olmadığı esasına dayanır. Bu nedenle kontrolcü ve etkileştiği ortam pasif ise bileşke kararlılık garanti edilebilir. Neyse ki pasif ortamlar kütlelerin, yayların ve sönümleyecilerin doğrusal veya doğrusal olmayan tüm kombinasyonlarını içeren kapsamlı ve kullanışlı bir küme oluşturur. Ayrıca insan operatörler de pasif bir ağ elemanı olarak incelenebilir. Pasiflik paradigması, gürbüz kararlılık ve kontrolcü tasarım kolaylığı sağladığından fİRE uygulamaları için caziptir. Bununla birlikte, pasiflik kontrolcüye performansı düşüren katı sınırlamalar getirdiği için kısıtlayıcı bir paradigmadır. Bu nedenle kontrolcü tasarımı için en geniş pasiflik sınırlarını elde etmek çok önemlidir.

Seri elastik eyleme (SEE) fİRE uygulamaları için önemli avantajlar sağladığından yaygınlaşmıştır. SEE, eyleyici ve yük arasına bilinçli olarak esneklik eklemek suretiyle geleneksel eyleyicilere göre daha kaliteli kuvvet kontrolü ve gürbüz kararlılık sağlar. Literatürde SEE için çeşitli empedans kontrol mimarileri sunulmuştur. Bu alternatifler arasında en içte hareket kontrolcüsü, ortada kuvvet kontrolcüsü ve en dışta empedans kontrolcüsünden oluşan kademeli kontrol mimarisi basitlik, gürbüzlük ve performans açısından cazip ve yaygındır.

Bu tezde, iki klasik doğrusal empedans modeli olan sıfır empedans ve saf yayı kademeli SEE empedans kontrol mimarisi ile pasif olarak gerçeklemek için gerekli ve yeterli koşulları türettik. Yeni bulduğumuz pasiflik koşullarına dayanarak kısıtlayıcı

olmayan kontrolc tasarımları sunduk. Bu yönergeler haptik olarak boş uzay ve sanal yay gerçeklerken bileşke kararlılığı ve dolayısıyla etkileşim güvenliğini korumaktadır. Bu pasiflik koşullarının doğruluğunu bilgisayar benzetimleri ve fiziksel deneyler ile gösterdik.

İntegral denetleyicilerinin kullanıldığı mimarilerde pasiflik koşulları türetilirken fiziksel sönümleyicinin eyleyici modeline dahil edilmesinin önemini de ayrıca gösterdik. Sönümleyicinin pasiflik sınırlarına fazladan bir kısıtlama getirdiğini saptadık. Böylece eyleyici sönümlemesinin sistemin pasifliğine sezgisel olmayan olumsuz etkisini vurguladık .

SEE yapısına ek olarak seri elastik sönümlenmiş eylemeyi (SESE) inceledik ve kademeli SEE'nin pasif olarak gerçekleştiremediği empedansları kademeli SESE'nin gerçekleştirebildiğini gösterdik. Özellikle SESE'nin Voigt modeli ve hatta fiziksel yay-sönümleyici çiftinden daha sert empedansları pasif olarak gerçekleştirebildiğini matematiksel analizler ve benzetimler ile doğruladık.

« Aileme, dostlarıma ve ilk bilim adamı
El-Hasan İbn-i Heysem'e »

ACKNOWLEDGEMENTS

Humans are social animals! Fruitful research stems from interactions with several contributors. Therefore, I would like to acknowledge those who have played an important role in making this thesis possible.

The opening part of the eternal sonnet named research comes from advisors. I am blessed to have Prof. Volkan Patođlu as the composer of the intro. His guidance, kindness, support, scientific insights, and work ethics have aspired me to be an ambitious and diligent researcher. I sincerely wish that I will live up to his standards and expectations throughout my academic journey.

For this thesis, I would like to thank my committee members: Prof. ađatay Bařdođan and Prof. Kemalettin Erbatur for their time, interest, and insightful questions and helpful comments to fulfill the potential of this work.

I also wish to express my thanks to Prof. Mustafa Unel, whose teaching and guidance have broadened my vision. His rigor and passion for control theory and applied mathematics have been a great inspiration source for my research framework.

I am particularly thankful for the wonderful (passive) environment in Human-Machine Interaction (HMI) lab at Sabanci University. They are all surely contributors of this thesis with their insightful questions and comments during the regular lab meetings. Special thanks to Mahmut Beyaz for his phenomenally thought-provoking questions which made this work reach at a climax.

Out of all the HMI group members, I wish to express special thanks to Umut alıřkan for being kind enough to share his experimental setup and know-how with me for the experimental validation of this work. Without him, the world would have required to wait for another year for this exceptional work on the passivity of series elastic actuators.

I wish to express special thanks to my dear roommate Ali Khalilian Bonab and dear friend Vahid Tavakoli for all the amazing fun and adventure we had together as three post-graduate bachelors. Pun was indeed intended.

I want to thank Zeynep Özge Orhan, and Uğur Mengilli for their friendship and unconditional support throughout my studies. I also want to thank my colleagues from different labs in the mechatronics department. In particular, I wish to express my sincere gratitude to Gökhan Alcan Ph.D. for being an enthusiastic teaching assistant. I feel lucky to have him as my teaching assistant for several undergraduate and graduate courses. I genuinely appreciate Mehmet Emin Mumcuoğlu, Diyar Bilal, Naida Fetic, and Hande Karamahmutoğlu for their friendship and help.

Not last but definitely the least I want to thank my brother from another mother Zain Fuad for his unconditional support and friendship. Without him, I would still live my life, but his presence surely makes my life more awesome. I am blessed to know him.

Last but foremost, I want to thank my family for their constant, unwavering support, and understanding. None of my achievements would have been possible without them. I would like to express special thanks to my dad Murat Tosun for setting a great example as an academician. I want to thank my mom Emine Tosun for all her sacrifices to raise me. I also want to thank my brother Barış Efe Tosun, who is the joy of our family. I am glad to have them in my life.

Table of Contents

Abstract	iii
Özet	v
Acknowledgements	viii
Table of Contents	x
List of Figures	xi
List of Tables	xii
1 Introduction	1
1.1 Motivation	1
1.2 Contributions	6
1.3 Outline	8
2 Literature Review	9

3	Preliminaries	13
3.1	Passivity Framework as a Solution to the Problem of Coupled Stability	13
3.2	Uncontrolled Series Elastic Actuation	15
3.3	Impedance as a Quantitative Measure of Mechanical Interaction . . .	16
4	Passivity Analysis of Impedance Controlled Velocity Sourced SEA	18
4.1	System Description	18
4.2	Passivity Analysis	20
4.2.1	Null Impedance Rendering	21
4.2.2	Pure Spring Rendering	27
4.3	Discussion	32
5	Analysis of Rendering Fidelity	37
5.1	Effects of Controller Gains on Null Impedance Rendering	38
5.1.1	Design Guidelines for Null Impedance Rendering	42
5.2	Effects of Controller Gains on Pure Stiffness Rendering	42
5.2.1	Design Guidelines for Pure Stiffness Rendering	46
5.3	Overall Design Guidelines	47
6	Experimental Validation	48
6.1	System Identification	49
6.2	Torque Controller Tuning	53
6.3	Impedance Rendering Performance	55

6.3.1	Pure Spring Rendering	55
6.3.2	Null Impedance Rendering	57
6.4	Experimental Verification of Passivity Bounds	59
7	Series Elastic Damping Actuation (SEDA)	62
7.1	Impedance Control of Velocity Sourced Series Elastic Damping Actuation (SEDA)	63
7.1.1	Rendering Null Impedance	66
7.1.2	Rendering Pure Springs	68
8	Conclusions and Future Work	71
	Bibliography	73

List of Figures

3.1	Mechanical schematics of a series elastic actuator	15
3.2	Block diagram of an uncontrolled series elastic actuator	16
4.1	Velocity-force cascaded control of a series elastic actuator	18
4.2	The effect of actuator damping on system passivity	35
5.1	Null impedance rendering with various velocity proportional gains . .	39
5.2	Null impedance rendering with various velocity integral gains (I_m) . .	40
5.3	Null impedance rendering with various torque proportional gains P_t .	40
5.4	Null impedance rendering with various torque integral gains I_t	41
5.5	Pure spring rendering with various velocity proportional gains P_m . .	43
5.6	Pure spring rendering with various velocity integral gains I_m	44
5.7	Virtual spring rendering with various torque proportional gains P_t . .	45
5.8	Virtual spring rendering with various torque integral gains I_t	45
6.1	Experimental setup: SEA brake pedal	48
6.2	Closed loop motion controlled system	49
6.3	Experimental and simulated model output during system identification	50

6.4	Comparative bode plot of the real and reduced model	51
6.5	Chirp tracking reference tracking performance for a frequency range up to 4Hz	53
6.6	Set-point torque tracking reference tracking performance for 1 Nm, 2 Nm and 3 Nm	54
6.7	Experimental verification of rendering two virtual torsional springs with 20 Nm/rad and 40 Nm/rad stiffness	55
6.8	Human subject interacting with a hard virtual wall	56
6.9	Human subject interacting with a soft virtual wall	57
6.10	Human subject interacting with the device when it renders null impedance	58
6.11	Pt-It plot for experimentally testing coupled stability	61
6.12	Kd-It plot for experimentally testing coupled stability	61
7.1	Velocity-force cascaded control of a series damping elastic actuator . .	63
7.2	High impedance rendering with series elastic damping actuator	65
7.3	Low impedance rendering with series elastic damping actuator	66
7.4	Null impedance rendering with series elastic damping actuator	67
7.5	Stiff wall rendering with series elastic damping actuator	68
7.6	Pure spring rendering with series elastic damping actuator	69

List of Tables

4.1	The necessary and sufficient conditions for passivity when one integrator gain is set to zero	31
4.2	Design Guidelines for Rendering Null Impedance	32
4.3	Design Guidelines for Rendering Virtual Spring	33
4.4	34
5.1	Physical parameters considered for the SEA plant	37
5.2	Nominal controller gains to render null impedance	38
5.3	Nominal controller gains to render a pure spring	43
6.1	Identified parameters of the SEA brake pedal	52
6.2	Control parameters of the SEA plant for haptic impedance rendering	53
7.1	Simulation parameters for SEDA rendering Voigt model	65

Chapter 1

Introduction

1.1 Motivation

Ensuring natural and safe physical human-robot interactions (pHRI) is an active research area, since such interactions form the basis of successful applications in many areas, including service, surgical, assistive, and rehabilitation robotics. Safety of interaction requires the impedance characteristics of the robot at the interaction port to be controlled precisely [15]. Along these lines, many robot designs and several impedance control [29] schemes have been proposed.

Many successful applications rely on open-loop force/impedance control to avoid the use of force sensors. In these approaches, the motor torques/impedances are directly mapped to the end-effector forces/impedance. The performance of open-loop control approaches relies on the transparency of the mechanical design. In particular, the mechanical design of the robot needs to have high stiffness, low inertia, and high passive backdrivability to ensure good performance by minimizing parasitic forces. Optimization techniques exist to help design robots with high transparency [26, 59]. However, the design of highly transparent robots become quite challenging, even

infeasible, as high force/impedance levels are necessitated, since backdrivable high torque/power density actuators are not available.

Many robotic systems rely on closed-loop force control to compensate for parasitic forces originating from the mechanical design. However, the performance of closed-loop force controllers suffers from an inherent limitation imposed by the non-collocation of sensors and actuators. In particular, given that a force sensor needs to be attached to the interaction port, there always exists inevitable compliance between the actuators and the force sensor. This non-collocation results in a fundamental performance limitation for the controller, by introducing an upper bound on the loop gain of the closed-loop force-controlled system. Above this limit, the closed-loop system becomes unstable [3, 18].

When traditional force sensors with high stiffness are employed in the control loop, the stable loop gain of the system is mostly allocated for the force sensing element, and this significantly limits the upper bound available for the controller gains to achieve fast response and good robustness properties from the controlled system. Consequently, such force control architectures typically rely on high quality actuators/power transmission elements to avoid hard-to-model parasitic effects, such as friction and torque ripple, since these parasitic forces may not be effectively compensated by robust controllers based on aggressive force-feedback controller gains.

Series elastic actuation (SEA) trades-off force-control bandwidth for force/impedance rendering fidelity, by introducing highly compliant force sensing elements into the closed-loop force control architecture [30, 44]. By decreasing the force sensor stiffness, it allows higher force controller gains to be utilized for responsive and robust force-controllers. SEA can effectively mask the inertia of the actuator side from the interaction port, featuring favorable output impedance characteristics that is safe for human interaction over the entire frequency spectrum. In particular, by modulating its output impedance to a desired level, SEA can ensure *active* backdrivability,

within the force control bandwidth of the device, through closed-loop impedance control of high power density actuators. For the frequencies over its control bandwidth, the apparent impedance of the system is limited by the inherent compliance of the force sensing element that acts as a physical filter against impacts, impulsive loads, and high frequency disturbances [30, 44, 46, 51].

SEA is also preferred, since the cost of SEA robotic devices can be made significantly (about an order of magnitude) lower than traditional force sensor based implementations, as successfully demonstrated by the commercial Baxter robot [1]. In particular, since the orders of magnitude more compliant force sensing elements in SEA experience significantly larger deflections with respect to commercial force sensors, regular position sensors, such as optical encoders, can be employed to measure these deflections, enabling the implementation of low-cost digital force sensing elements that do not require signal conditioning. Furthermore, since the robustness properties of the force controllers enable SEA to effectively compensate for parasitic forces, lower cost components can be utilized as actuators/power transmission elements in the implementation of SEA. To date, a large number of SEA designs have been developed for a wide range of applications [9, 19, 20, 35, 37, 42, 44, 46, 48, 50, 52, 62, 66, 68].

The main disadvantage of SEA is the significantly decreased closed-loop bandwidth caused by the increase of the sensor compliance [44]. The determination of appropriate stiffness of the compliant element is an important aspect of SEA designs, where a compromise solution needs to be reached between force control fidelity and closed-loop control bandwidth. In particular, higher compliance can increase the force sensing resolution, while higher stiffness can improve the control bandwidth of the system. Possible oscillations of the end-effector, especially when SEA is not in contact, and the potential energy storage of the elastic element may pose as other challenges of SEA designs, depending on the application.

SEA is a multi-domain concept whose performance synergistically depends on the design of both the plant and the controller [31, 32]. The high performance controller design for SEA to be used in pHRI has further challenges, since ensuring safety of interactions is an imperative design requirement that dominates the design process. In particular, the safety of interaction requires coupled stability of the controlled SEA together with the human operator. However, the presence of a human operator in the control loop significantly complicates the stability analysis, since a comprehensive model for human dynamics is not available. Particularly, human dynamics is nonlinear, time and configuration-dependent. Contact interactions with the environment pose similar challenges, since the impedance of the contact environment is, in general, nonlinear and uncertain.

The coupled stability analysis of the pHRI system in the absence of human and environment model is commonly conducted using the frequency domain passivity framework [13, 14]. This approach assumes that the human operator is cooperative and does not intentionally generate energy to destabilize the system, that is, the intentional part of human inputs are state independent while the unintentional parts are passive by nature. Under this assumption, the human can be treated as a passive network element in the closed-loop analysis, and coupled stability can be concluded through passivity arguments [28]. Similarly, non-animated environments are also passive. Therefore, coupled stability of the overall system can be concluded, if the closed-loop SEA with its controller can be guaranteed to be passive [12]. Passivity framework is advantageous as it provides robust stability for a large range of human and environment models. However, non-passive systems are not always unstable [6] and the passivity is a relatively conservative condition that imposes strict constraints on the controller gains to degrade the system performance.

It is well-established that ensuring passivity adversely affects the transparency [36], and this trade-off brings a challenge in the design of high-performance controllers that can ensure coupled stability. The trade-off between stability and transparency [16,

21, 24], as well as the factors affecting the transparency have been investigated in the literature [27, 49, 55]. While keeping coupled stability intact, a controller allowing better compromise between transparency and robust stability is desirable [49].

1.2 Contributions

In this thesis, we analyze the well-known cascaded control architecture for impedance controlled series elastic actuation with an inner-most velocity loop, an intermediate torque loop, and an outer-most impedance loop whose effectiveness was reported in earlier studies. This cascaded architecture is also termed as velocity sourced SEA. We utilize the frequency domain passivity framework to ensure the coupled stability of the system when interacting with a human operator or a passive environment. This framework provides a mathematical guarantee for the safety of interaction.

Contributions of the thesis may be summarized as follows:

- We derive the *necessary and sufficient conditions* for the passivity of haptic rendering of null impedance and pure spring with the velocity sourced SEA scheme and non-negative control gains. Based on the newly established passivity bounds, we provide non-conservative design guidelines to haptically display free-space and virtual springs.
- Our results rigorously extend the earlier reported sufficiency conditions on the passivity of this particular SEA scheme and provide the least conservative range for passively renderable impedances. Since passivity is a conservative paradigm that imposes stringent limits on control gains which degrade the performance, it is of paramount importance to come up with the most relaxed passivity conditions to allow flexibility in controller gain selection to maximize the performance.
- Our results remark the importance of including physical damping in the actuator model for passivity analysis, especially when integrators are utilized. Earlier works in the literature tend to model the motor side of the SEA as pure inertia, thus disregard the damping term, which is always present for

any physical system. This is due to the presumption that additional damping would never violate passivity due to its dissipative nature. Hence, the passivity bounds derived for the simplified SEA model was intuitively expected to extend to the realistic scenario where physical damping is also present. We rigorously rebut this conjecture and prove that the damping term introduces an extra passivity bound on control gains.

- Through the derivation of necessary and sufficient conditions, we have established the need for an integrator in the inner velocity loop to be able to passively render a virtual spring.
- We analyze haptic impedance rendering of series elastic damping actuation (SEDA) which has a linear spring-damper in parallel as the compliant force-sensing element. We demonstrate its capability of passively rendering Voigt model, which is a parallel spring-damper. This is a useful extension to velocity sourced SEA as it was early proven that the cascaded control of SEA cannot render Voigt body passively.
- We prove that SEDA can passively render higher virtual impedances than the physical impedance of the compliant element. The maximum passively renderable stiffness is bounded from above by the stiffness of the physical spring employed in the regular SEA. However, rendering fidelity of SEDA is low for null impedances and pure springs as the physical damping starts to dominate the interaction at relatively low frequencies.

1.3 Outline

The rest of the thesis is organized as follows.

Chapter 2 reviews the related work and emphasizes the contributions of this paper in comparison to the related works.

Chapter 3 presents the preliminaries to build the necessary background for the problem of coupled stability, the concept of SEA in force control, and the frequency domain passivity framework for linear 1-port networks.

Chapter 4 explains the controlled system considered in this study and lists the underlying assumptions together with their justification. It also derives the necessary and sufficient conditions for passivity while rendering null impedance and pure springs.

Chapter 5 systematically studies the rendering performance with respect to the controller gains via simulation. It also provides detailed controller design guidelines.

Experimental verification with a series elastic actuated brake pedal is performed in Chapter 6.

Chapter 7 scrutinizes SEDA as a possible extension to SEA and presents discussion about potential benefits and drawbacks.

Chapter 8 concludes the paper and discusses the future research directions.

Chapter 2

Literature Review

In this section, we review related works on force/impedance controlled SEA and explain how our work extends the earlier studies.

The notion of intentionally introduced compliance between the actuator and the end effector for force controlled robotic joints has been first proposed in [30]. Later, the term “series elastic actuator” (SEA) was coined for this force control scheme and passivity analysis was conducted for the first time in [44] which has popularized the concept among roboticists. A minor difference between the implementations in [30] and in [44] is that the former performs subtraction on the position measurements of the motor and the end effector to obtain the spring deflection while the latter directly measures it to reduce the noise in measurements.

The SEA controller in [44] is based on a single force-control loop, where the actuator is torque controlled based on the deflection feedback from the compliant element. Similarly, a PID controller with feed-forward acceleration terms to compensate the actuator inertia has been proposed in [46]. These early strategies rely on low-pass filters instead of pure integrators to preserve passivity, at the expense of allowing steady state errors under constant disturbances.

Other control techniques for SEA include disturbance observer based force controllers [35, 43] and controllers based on high order derivatives [2]. While linear models are most widely adapted for force/torque control of SEAs, there also exist some nonlinear control strategies [7, 33, 41, 63].

A fundamentally different architecture based on cascaded control loops has also first been proposed in [30] and later rediscovered in [45, 67]. In this approach, an inner-loop controls the velocity of the actuator, rendering the system into an “ideal” motion source, while an outer-loop controls the interaction force based on the deflection feedback from the compliant element. Wyeth called this approach *velocity-sourced SEA* [67], emphasizing that most of the earlier work considered the motor as a torque source rather than a velocity source. Wyeth’s implementation slightly differs from [30] and [45] in that he utilizes noncollocated sensor measurements (i.e., the deflection of the spring) in the control loop while the others use the collocated measurements (i.e., the position of the motor). This particular strategy allows for the use of integrators; thus the closed-loop controlled system can effectively counteract constant disturbances at the steady state. This architecture also allows for utilization of well-established robust motion controllers for the inner-loop to counteract parasitic effects of friction and stiction. Furthermore, the controller can be tuned easily without the need for precise actuator dynamics. The cascaded control approach has been widely utilized in various applications [9, 19, 37, 42, 48, 52, 56, 62].

Using the cascaded control architecture, Vallery *et al.* derived and experimentally verified *sufficient conditions* to ensure passivity of the impedance rendering, for the case of zero reference torque [60]. They have suggested simple yet quite conservative guidelines: select a proportional velocity gain that is greater than the motor inertia, and select integrator gains that are less than the half of the corresponding proportional gains. In their later work, Vallery *et al.* conducted a theoretical analysis and an experimental study for pure spring rendering [61]. In this work, it has been

proven that, for the cascaded control architecture, the passively renderable virtual stiffness is bounded by the stiffness of physical spring employed in the SEA.

For a variety of viscoelastic virtual impedance models, Tagliamonte *et al.* performed a theoretical analysis using the cascaded control architecture, but also including the damping coefficient in the actuator dynamics [54]. In this work, they have proposed less conservative *sufficient conditions* to ensure passivity with properly selected controller gains, for the cases of null impedance and pure spring rendering. They have also demonstrated that the Voigt model, that is, linear spring and damping elements in parallel connection, cannot be passively rendered using the cascaded control architecture.

Recently, Fiorini *et al.* surveyed different impedance and admittance control architectures for SEA and summarized *sufficient conditions* for passive impedance rendering with basic impedance control, velocity-sourced impedance control, collocated admittance control and collocated impedance control architectures [8]. This study concludes that similar bounds on passively renderable impedances exist for all four control architectures and these limits can be extended, if ideal acceleration feedback can be used to predict and cancel out the influence of load dynamics. Noise and bandwidth restrictions of acceleration signals and potential overestimation of feed-forward signals resulting in feedback inversion are important practical challenges that have limited the adaptation of the acceleration-based control approach since initially proposed in [44, 46].

This work builds upon earlier works on passivity of velocity-sourced impedance control of series elastic actuators [54, 60, 61] and extends their results by providing the *necessary and sufficient conditions* to ensure passive rendering of null impedance and pure springs. Our results not only provide rigorous sufficiency proofs, but also relax the earlier established bounds by extending the range of impedances that can be passively rendered via cascaded control architecture. Based on the newly

established necessary and sufficient conditions, design guidelines are provided to select controller gains to reach optimal performance while maintaining passivity.

Furthermore, our results prove the *necessity* of a second bound on the integral gains due to existence of physical damping in the system. This bound has been overlooked in the literature [60, 61], as it is counter-intuitive for additional dissipation to result in more strict conditions on controller gains. However, this bound is crucial in practice, as it is imposed due to inevitable physical dissipation of the actuator; hence, cannot be safely neglected, if integral controllers are used in both inner motion and intermediate torque control loops. We also remark that the damping term counterintuitively reduces the Z-width of the system, that is, the dynamic range of passively renderable impedances, as also reported in [54].

Chapter 3

Preliminaries

In this chapter, the reader will be provided with the preliminary information for the forthcoming analyses. In particular, the frequency domain passivity framework will be motivated within the context of pHRI following the introduction of the problem of coupled stability. Finally, this chapter concludes with the linear time-invariant model of uncontrolled series elastic actuation.

3.1 Passivity Framework as a Solution to the Problem of Coupled Stability

Stability is an imperative criterion for any control system to maintain the safety of operation. The stability of any LTI system can easily be assessed with the Routh-Hurwitz criterion. Therefore, it is easy to tune the control parameters to ensure the stability of an LTI system. However, when two systems that are stable in isolation are coupled to each other, there is no guarantee that the coupled system will also be stable. This makes the control design problem challenging when the controlled

system needs to interact with an environment whose dynamics are unknown (e.g., human). This is known as the problem of coupled stability.

Intuitively, a system is said to be passive if and only if the total energy stored in the system is greater than or equal to total energy supplied out to the environment at any time instant. The coupled stability is guaranteed for any two passive (regardless of linearity and shift invariance) and detectable system. Since the detectability condition is satisfied in most cases, passivity is an appealing paradigm for stability robustness.

Theorem 1 (Passivity of a linear 1-port network [15]). An LTI and single-input single-output (SISO) system, whose transfer function is denoted as $H(s)$ is passive if and only if the following conditions hold:

- (i) $H(s)$ must have all its poles in the open left half plane.
- (ii) $Re\{H(jw)\} \geq 0$ for all $w \in (-\infty, \infty)$ for which jw is not a pole of $H(s)$.
- (iii) Poles on the imaginary axis are allowed only if they are simple and have positive real residues.

Condition (i) implies (isolated) stability, but all three conditions are required to be simultaneously satisfied for passivity.

In this section, we presented an informal definition of passivity and motivated the usage of passivity framework for pHRI applications. We also provided a mathematical definition for the frequency domain passivity of LTI SISO systems. More general definitions are available in the literature but beyond the scope of our study.

3.2 Uncontrolled Series Elastic Actuation

Figure 3.1 depicts the model of a 1-DOF linear SEA. In particular, the motor side consists of a linear mass-damper and connects to the load (i.e., the end-effector) via a linear spring of stiffness K . F_m represents the forces exerted on the motor and F_h represents the forces exerted on the end-effector by the human operator. The inertia of the motor side is denoted as M while the inertia of load side is denoted as m which is typically orders of magnitude smaller than M . x_m denotes the position of the motor while x_e is the end-effector position. Assuming a rigid contact between the human operator and the end-effector, we obtain the following relationship $x_e = x_h$, where x_h is the exogenous input to the system by the user interaction. The equations of motion for this simple system read as follows:

$$F_m = M\ddot{x}_m + b\dot{x}_m + K(x_m - x_e) \quad (3.1)$$

$$F_h = Z_e\dot{x}_e - K(x_m - x_e) \quad (3.2)$$

$$F_s = K(x_m - x_e) \quad (3.3)$$

where Z_e represents the overall impedance of the load side and F_s is the force on the spring. The control diagram of the uncontrolled SEA plant may be obtained as in Figure 3.2 after taking the Laplace transform of the equations above and simple algebraic manipulations.

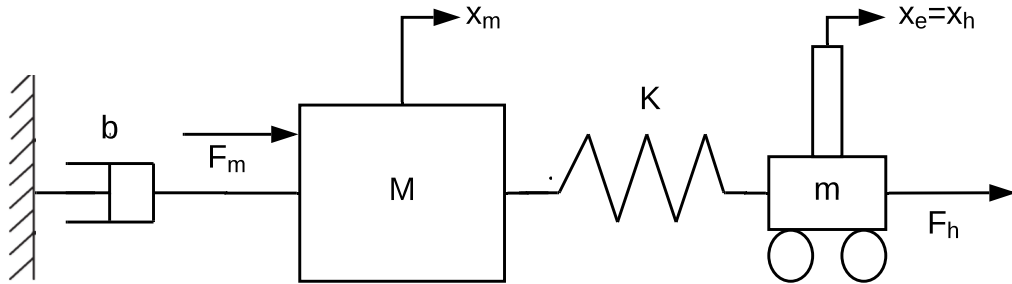


FIGURE 3.1: Mechanical schematics of a series elastic actuator

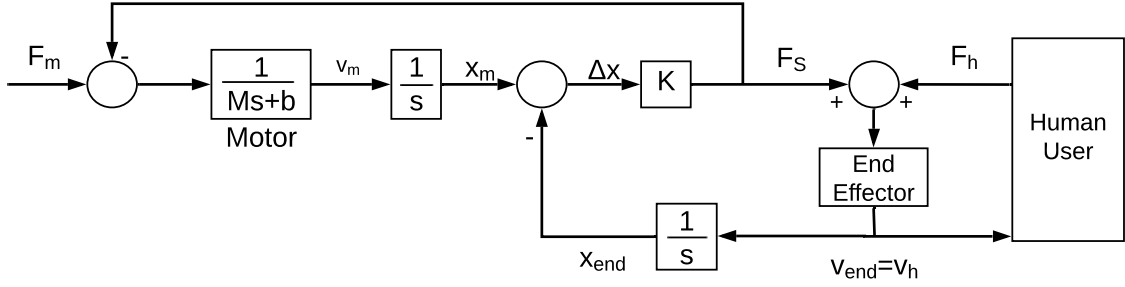


FIGURE 3.2: Block diagram of an uncontrolled series elastic actuator

The deliberately introduced compliance between the motor and the end-effector creates a natural feedback loop as can be seen figure 3.2. Note that the signals depicted in this block diagram are all physical.

It takes a simple step to build a force-controlled SEA from the uncontrolled SEA plant. In particular, an outer force controller (typically a PI compensator) is added to the system. The output force can easily be estimated by the product $K\Delta x$ and fed back to create a closed-loop system.

Similarly, to build an impedance-controlled SEA, an outer impedance loop through position feedback is closed around the force-controlled SEA. Note that in this case, the purpose of the outermost loop is to regulate the output impedance seen from the human side. It achieves its goal by creating reference signals to the force controller to render a desired virtual environment.

3.3 Impedance as a Quantitative Measure of Mechanical Interaction

This section gives the mathematical definition of the impedance operator to quantify the interaction between the robot and environment. In particular, mechanical impedance (denoted as Z) is a dynamic operator (not necessarily linear) that maps

an input velocity to an output force as a function of time at the interaction port. An interaction port is the interface where the energy exchange with the environment (or another controlled system) takes place. The energy exchange is quantified in terms of the conjugate flow and effort variables such that $P = F^T v$, where F is a vector of forces along different degrees of freedom, v is the corresponding velocity vector and P is the power flow between robot and environment. The mechanical impedance seen from the robot side at the interaction port is also termed as the *driving point impedance*.

Impedance may conveniently be represented in the Laplace domain by a transfer function $Z(s)$ for LTI 1-port systems. For LTI n-port systems, impedance may be represented as a matrix of transfer functions. Since our analysis will be restricted to an LTI single degree-of-freedom SEA, the output impedance (or the driving point impedance) function can be expressed as $Z(s) = \frac{F(s)}{V(s)}$. For instance, the impedance of a mass-spring-damper is equal to $Z(s) = ms + b + K/s$, where m is the inertia of the mass, b is the damping coefficient, and K is the spring stiffness.

Chapter 4

Passivity Analysis of Impedance Controlled Velocity Sourced SEA

This chapter rigorously derives the necessary and sufficient conditions for passivity when rendering null impedance and pure springs with velocity-sourced SEA.

4.1 System Description

Figure 4.1 depicts the block diagram of velocity-sourced impedance control for SEA. In particular, the cascaded controller is implemented with an inner motion control loop to render the system into an ideal motion source, and the outer force/torque

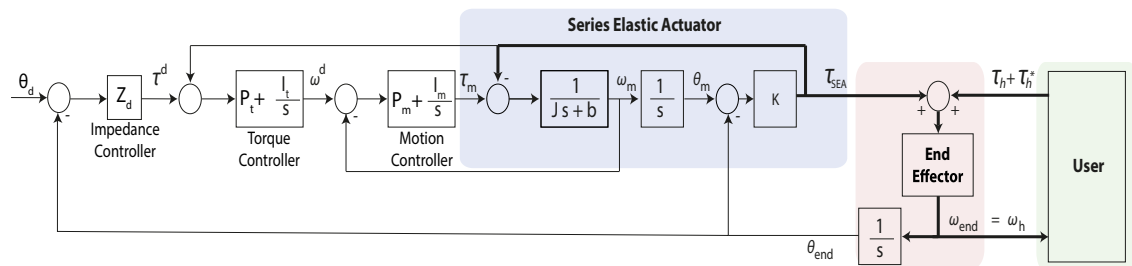


FIGURE 4.1: Velocity-force cascaded control of a series elastic actuator

control loop generates references for the motion control loop such that the spring deflection is kept at the desired level to match the reference force. The interaction torque is measured through the linear spring torque that is proportional to the difference between motor position θ_m and end-effector position θ_{end} . The interaction forces τ_{SEA} and τ_h are denoted with thick lines.

Note that, the physical spring torque acts as a disturbance to the motion controller while the measured torque (denoted with a thin line) is feedback to the outer torque controller. τ_h represents the unintentional torques from the human which are inherently passive. τ_h^* represents the intentional torques which are state-independent and do not affect the coupled stability.

The dynamics of the SEA model consist of actuator inertia J , viscous friction b , and the linear spring constant K . PI controllers are employed for both velocity and torque control loops. At the outermost loop, an impedance controller is employed to generate references to the torque controller depending on the desired impedance Z^d to be displayed around the equilibrium position of the virtual environment θ^d .

Some simplifying assumptions are considered while developing the SEA model and its control architecture, as in [54]. These assumptions include:

- To develop a linear time-invariant (LTI) model, nonlinear effects like stiction, backlash and motor saturation are neglected. In the literature, it has been demonstrated that the cascaded force-velocity control scheme can effectively overcome the problems of stiction and backlash [50, 67]. If the motor is operated within its linear range, then the other nonlinear effects like motor saturation also vanish.
- The overall inertia and damping of the SEA are considered to be on the motor side. The inertia of the load is not included in the analysis, since the load inertia does not contribute to the passivity conditions.

- Electrical dynamics of the system is neglected based on the commonly employed assumption that electrical time constant of the system is orders of magnitude faster than the mechanical time constant.
- It is assumed that motor velocity signal is available with a negligible delay. This assumption is realistic for electronically commuted motors furnished with Hall effect sensors. Furthermore, for motors furnished with high-resolution encoders, differentiation filters running at high sampling frequencies (commonly on hardware) can be employed to result in real-time estimation of velocity signals with very small delay, within the bandwidth of interest.
- Without loss of generality, for simplicity of analysis, zero reference trajectory is assumed for the equilibrium position (i.e. $\theta^d = 0$) and transmission ratios are set to unity.

Conventionally, the output impedance Z_{out} of the closed loop system is defined at its output port as the relationship between the conjugate variables $\omega_{end}(s)$ and $\tau_{SEA}(s)$ as

$$Z_{out} = -\frac{\tau_{SEA}(s)}{\omega_{end}(s)} = -\frac{\tau_{SEA}(s)}{s\theta_{end}(s)} \quad (4.1)$$

The minus sign comes from the convention that the output torque (i.e., torque on the spring) is taken positive when the spring is in compression. The following analysis is performed based on Eqn. (4.1) as it defines the relationship at the interaction port of the human/environment and the end-effector of SEA.

4.2 Passivity Analysis

The necessary and sufficient conditions for the passivity of the system depicted in Figure 4.1 for positive system parameters and control gains are derived by using Theorem 1 in Section 3.1.

4.2.1 Null Impedance Rendering

Let us first analyse the case of null impedance (i.e $Z_d=0$), which also corresponds to the special case where the outer-most impedance loop is cancelled and zero set-point reference signal is fed to the torque controller (i.e $\tau^d = 0$). This particular case is interesting as it is commonly employed to ensure the active backdrivability of SEA. From Eqn. (4.1), the output impedance is expressed as

$$Z_{out}^{null} = \frac{K s (J s^2 + (P_m + b) s + I_m)}{D_Z(s)} \quad (4.2)$$

where

$$D_Z(s) = J s^4 + (P_m + b) s^3 + (K + \gamma) s^2 + \alpha K s + K I_m I_t \quad (4.3)$$

with $\alpha = P_m I_t + P_t I_m$ and $\gamma = K P_m P_t + I_m$.

Let us determine the controller gains that guarantee passivity. Naturally, the parameters J and b that capture the motor dynamics and the spring constant K are always positive. It is established in classical control theory that if any one of the coefficients of the characteristic equation is non-positive in the presence of at least one positive coefficient, then the system is unstable [40]. Along these lines, we also assume that all controller gains are selected as positive. This selection satisfies the necessary condition for the stability of the system.

The method of Hurwitz determinants or Routh's stability criterion can be used to assess the stability of a system, which is the first condition for it to be passive. The Routh array of a fourth order system with a characteristic equation of the form $a_0 s^4 + a_1 s^3 + a_2 s^2 + a_3 s + a_4$ reads as

a_0	a_2	a_4
a_1	a_3	0
$(a_1 a_2 - a_0 a_3)/a_1$	a_4	0
$(a_1 a_2 a_3 - a_1^2 a_4 - a_0 a_3^2)/(a_1 a_2 - a_0 a_3)$	0	0
a_4	0	0

It follows from the Routh array that the following two inequalities need to be satisfied to ensure stability.

$$a_1 a_2 - a_0 a_3 > 0 \tag{4.4}$$

$$a_1 a_2 a_3 - a_0 a_3^2 - a_4 a_1^2 > 0 \tag{4.5}$$

Note that if Eqn. (4.5) is satisfied, then Eqn. (4.4) is also met, as can be proven by multiplying Eqn. (4.4) with a_3 , and noting that Eqn. (4.5) ensures that $a_1 a_2 a_3 - a_0 a_3^2 > a_4 a_1^2 > 0$. Hence, if we define a variable as $\xi := a_1 a_2 a_3 - a_0 a_3^2 - a_4 a_1^2$ the system is stable if and only if $\xi > 0$. The value of ξ in terms of our system parameters reads as

$$\xi = \alpha K (P_m + b)(K + \gamma) - K I_m I_t (P_m + b)^2 - J K^2 \alpha^2 \tag{4.6}$$

The inequality $\xi > 0$ represents Condition (i) of Theorem 1 for passivity. As for Condition (ii), we have to assess the positive-realness of $Z_{out}^{null}(jw)$. It is relatively involved to examine the positive-realness of a complex fraction directly. Along these lines, we use a polynomial that provides us with the same information about the sign of the real part of $Z_{out}^{null}(jw)$. There are multiple ways to obtain this polynomial [25]. For completeness of the presentation, below we provide one way to calculate this polynomial with the proof.

Proposition 1. For ease of notation, denote the frequency response of a SISO LTI system as $H(jw) = \text{num}(jw)/\text{den}(jw)$. Then, $\text{sign}(\text{Re}\{H(jw)\}) = \text{sign}(P(w))$ for

any value of w for which $\text{den}(jw) \neq 0$, where $\text{sign}(\cdot)$ represents the signum function and $P(w)$ is a polynomial defined as $P(w) = \text{Re}\{\text{num}(jw)\text{den}(-jw)\} = \sum_i d_i w^i$.

Proof. Multiply numerator and denominator of $H(jw)$ with the complex conjugate of the denominator as

$$H(jw) = \frac{\text{num}(jw)}{\text{den}(jw)} = \frac{\text{num}(jw)\text{den}(-jw)}{\text{den}(jw)\text{den}(-jw)} = \frac{\text{num}(jw)}{|\text{den}(jw)|^2}$$

Since the denominator of the resulting fraction is never negative and is zero only when $\text{den}(jw)$ is zero, we conclude that the proposition holds. \square

Consequently, $P(w) \geq 0$ is a necessary and sufficient test to ensure Condition (ii) for passivity. For the system described by Eqn. (4.2), $P(w)$ evaluates to

$$P(w) = d_2 w^2 + d_4 w^4 \quad (4.7)$$

where the coefficients are defined as

$$d_2 = K^2(P_t I_m^2 - b I_t I_m) \quad (4.8)$$

$$d_4 = K^2(P_m + b + P_t P_m^2 + b P_t P_m - J\alpha) \quad (4.9)$$

It will be proven that $d_2 \geq 0 \wedge d_4 \geq 0$ is a necessary and sufficient condition to ensure $P(w) \geq 0$ for $\forall w \in \mathbb{R}$

Proof. Sufficiency. Since there are only even powers of w in $P(w)$, the image of $P(w)$ is non-negative if all coefficients are also non-negative. \square

Proof. Necessity. Rearrange Eqn. (4.7) as $P(w) = w^2 (d_2 + d_4 w^2)$. Then, $P(w) \geq 0$ for $w \in (-\infty, \infty)$ if and only if $d_2 + d_4 w^2 \geq 0$. The roots to this simple quadratic expression (i.e., $d_2 + d_4 w^2$) are equal to $\pm \sqrt{-d_2/d_4}$.

If the signs of d_2 and d_4 agree, there is no real root to this expression, meaning that its graph never crosses the horizontal axis. Thus, if d_2 and d_4 are positive, then the graph has to lie above the abscissa for all w values. On the other hand, if the coefficients have opposite sign, there will be two real roots forcing the parabola to cross the abscissa and go below zero. In this case, $P(w)$ is negative for $w \in (-\sqrt{-d_2/d_4}, \sqrt{-d_2/d_4})$.

Finally, in the extreme case where either coefficient is zero the other coefficient must be greater than or equal to zero for $P(w)$ to be non-negative. \square

Thus, $P(w) \geq 0 \iff d_2 \geq 0 \wedge d_4 \geq 0$. Consequently, the *necessary and sufficient conditions* for the passivity of the system whose closed-loop impedance is characterized by Eqn. (4.2) can be expressed as follows:

$$\xi = K[\alpha(P_m + b)(K + \gamma) - I_m I_t (P_m + b)^2 - JK\alpha^2] > 0 \quad (4.10)$$

$$d_2 = K^2 [I_m (P_t I_m - b I_t)] \geq 0 \quad (4.11)$$

$$d_4 = K^2 [(P_m + b)(1 + P_m P_t) - J\alpha] \geq 0 \quad (4.12)$$

Proposition 2. The necessary and sufficient conditions to passively render zero impedance (or equivalently zero force/torque) for the cascaded controlled SEA shown in Figure 4.1 with positive control gains are as follows:

$$\left[J < \frac{(P_m + b)(1 + P_m P_t)}{P_m I_t + P_t I_m} \wedge b \leq \frac{P_t I_m}{I_t} \right] \quad (4.13)$$

\(\vee\)

$$\left[J \leq \frac{(P_m + b)(1 + P_m P_t)}{P_m I_t + P_t I_m} \wedge b < \frac{P_t I_m}{I_t} \right] \quad (4.14)$$

In the sequel, step-by-step proof is provided.

Lemma 4.1. $(d_2 \geq 0 \wedge d_4 > 0) \vee (d_2 > 0 \wedge d_4 \geq 0) \implies \xi > 0$

This statement implies that the Inequality (4.10) does not add extra restriction to the system of inequalities composed of Eqns. (4.10), (4.11) and (4.12), except that d_2 and d_4 cannot be zero simultaneously. In other words, d_2 and d_4 are non-negative, but only one of them can be zero at a time. Otherwise, the system is unstable.

The lemma contains two statements that are connected with the logical *or* operator. To facilitate understanding the discussion, the proof will be subdivided into these two parts.

Proof. *Part I: ($\mathbf{d}_2 \geq \mathbf{0} \wedge \mathbf{d}_4 > \mathbf{0}$).* Inequality (4.11) dictates an upper bound on b . According to Eqn. (4.11), the maximum value for the motor damping without violating passivity with the given controller gains can be computed as

$$b \leq \frac{P_t I_m}{I_t} = b_{max} \quad (4.15)$$

Inequality (4.12) dictates an upper bound on J . According to Eqn. (4.12), the maximum value for the motor inertia without violating passivity with the given controller gains can be computed as

$$J \leq \frac{(P_m + b)(1 + P_m P_t)}{P_m I_t + P_t I_m} = J_{max}^{null} \quad (4.16)$$

Now, assume the control gains are selected so that the motor inertia is less than its maximum allowable value. In other words, $J = J_{max}^{null} - \epsilon$ where $0 < \epsilon < J_{max}^{null}$. This selection entails $d_4 > 0$. After substituting this value of J in Eqn. (4.6), ξ becomes

$$\xi = \epsilon K^2 \alpha^2 + K I_m (P_m + b) (P_t I_m - b I_t) \quad (4.17)$$

Here, only the last term can make the expression negative, but this is avoided when Eqn. (4.15) is met. Thus, we conclude that $d_2 \geq 0 \wedge d_4 > 0 \implies \xi > 0$. \square

Proof. *Part II: ($\mathbf{d}_2 > \mathbf{0} \wedge \mathbf{d}_4 \geq \mathbf{0}$)*. Assume the control gains are selected so that the motor inertia takes its maximum allowable value that is, $J = J_{max}^{null}$. Substituting this value of J into Eqn. (4.6) yields the following expression.

$$\xi = K I_m (P_m + b) (P_t I_m - b I_t) \quad (4.18)$$

Clearly, ξ is positive if $J \leq J_{max}^{null}$ and $b < b_{max}$. Thus, passivity is ensured when $d_2 > 0$ and $d_4 \geq 0$. However, when $J = J_{max}^{null}$ and $b = b_{max}$ the value of ξ evaluates to zero, which implies instability. Thereby, the system is not stable when $d_2 = 0$ and $d_4 = 0$. \square

Consequently, $(d_2 \geq 0 \wedge d_4 > 0) \vee (d_2 > 0 \wedge d_4 \geq 0)$ constitutes the most general solution set that solves Eqns. (4.10), (4.11) and (4.12) concurrently, unless negative system parameters or controller gains are allowed. This concludes the proof of Proposition 2.

4.2.2 Pure Spring Rendering

In this section, we analyze the case where a virtual spring of stiffness K_d is displayed. When Z_d is set to K_d , the output impedance Z_{out}^{spr} reads as

$$Z_{out}^{spr} = K \frac{Js^4 + (P_m + b)s^3 + \delta s^2 + \alpha K_d s + K_d I_m I_t}{sD_Z(s)} \quad (4.19)$$

where $\delta = P_m P_t K_d + I_m$. The remaining intermediate parameters are the same as in the case of null impedance. Only a single pole located at the origin is added to the characteristic equation in Eqn. (4.3). Note that, this does not cause a violation of Condition (iii), since the pole on the imaginary axis is simple and have a positive residue as shown below.

$$\text{Res}_{s=0} Z_{out}^{spr} = \lim_{s \rightarrow 0} s Z_{out}^{spr} = \frac{K_d^2}{K} > 0$$

Therefore, Eqn. (4.10) for stability must also be adopted here.

The nonzero coefficients of $P(w)$ for this system are as follows:

$$d_4 = K[(K - K_d)\beta - \alpha K K_d] \quad (4.20)$$

$$d_6 = K[(K - K_d)\eta + K(P_m + b)] \quad (4.21)$$

where $\beta = P_t I_m^2 - b I_m I_t$ and $\eta = P_m^2 P_t + P_m P_t b - J \alpha$.

Note that, $P(w) \geq 0 \iff d_4 \geq 0 \wedge d_6 \geq 0$ as can be proven by rearranging $P(w)$ as $w^4(d_4 + d_6 w^2)$ and following the same reasoning as in the previous case. Thus, the necessary and sufficient conditions for the passivity of system whose closed-loop

impedance is characterized by Eqn. (4.19) are as follows

$$\begin{aligned}\xi &= K[\alpha(P_m + b)(K + \gamma) - I_m I_t (P_m + b)^2 - JK\alpha^2] > 0 \\ d_4 &= K[(K - K_d)\beta - \alpha K K_d] \geq 0\end{aligned}\quad (4.22)$$

$$d_6 = K[(K - K_d)\eta + K(P_m + b)] \geq 0 \quad (4.23)$$

Eqns. (4.22) and (4.23) stipulate some bounds on the renderable virtual stiffness. From Eqn. (4.22), we get the following upper bound for the renderable stiffness if $\beta + \alpha K$ is positive.

$$K_d \leq K \frac{\beta}{\beta + \alpha K} < K \quad (4.24)$$

Inequality (4.24) puts an upper bound on the physical damping. If β is negative, but $\beta + \alpha K$ is positive, then Eqn. (4.24) states that one cannot render a spring of any stiffness, since the maximum value for K_d would be a negative number. To ensure that $\beta > 0$, we need to employ the same bound on damping found in Eqn. (4.15). However, particular attention must be paid when $\beta + \alpha K$ is negative (in which case β is automatically negative). In this case, the controlled system becomes unstable as will be shown later. For the time being, we continue the analysis with the assumption of positive β (and hence positive $\beta + \alpha K$).

From Eqn. (4.23), we get the following upper bound for the renderable stiffness.

$$K_d \leq K \frac{\eta + P_m + b}{\eta} \quad (4.25)$$

Clearly, the value of K_d that satisfies Eqn. (4.24) also satisfies the less constraining inequality in Eqn. (4.25). Inequality in Eqn. (4.24) shows that if passivity is desired under the cascaded control architecture, the rendered stiffness must be strictly less than the stiffness of the physical spring employed in the SEA plant, which was originally reported in [61] excluding the damping term. Thus, the maximum value of the desired stiffness can be set to

$$\begin{aligned}
K_d^{max} &= K \frac{\beta}{\beta + \alpha K} \\
&= K \frac{P_t I_m^2 - b I_m I_t}{P_t I_m^2 - b I_m I_t + K(P_m I_t + P_t I_m)}
\end{aligned} \tag{4.26}$$

Proposition 3. The necessary and sufficient conditions to passively render a virtual spring for the system in Fig. 4.1 with positive control gains are

$$\left[J < \frac{(P_m + b)(\Delta K P_m P_t + K)}{\alpha \Delta K} \wedge b < \frac{P_t I_m}{I_t} \wedge K_d \leq K_d^{max} \right] \tag{4.27}$$

\(\vee\)

$$\left[J \leq \frac{(P_m + b)(\Delta K P_m P_t + K)}{\alpha \Delta K} \wedge b < \frac{P_t I_m}{I_t} \wedge K_d < K_d^{max} \right] \tag{4.28}$$

where $\Delta K := K - K_d$ and K_d^{max} is as in Eqn. (4.26).

Proof. From Eqn. (4.21),

$$d_6 = \Delta K (P_m + b)(\Delta K P_m P_t + K) - \Delta K J \alpha \geq 0 \tag{4.29}$$

Eqn. (4.29) introduces an upper bound on the motor inertia J as

$$J \leq \frac{(P_m + b)(\Delta K P_m P_t + K)}{\alpha \Delta K} = J_{max}^{spr} \tag{4.30}$$

Note that J_{max}^{spr} is not only a function of control gains, but also a function of the desired stiffness K_d to be rendered. If we set K_d to its maximum allowable value given in Eqn. (4.26), J_{max}^{spr} reads as

$$J_{max}^{spr} = \frac{(P_m + b)(P_t I_m^2 + \alpha K(1 + P_m P_t) - b I_m I_t)}{\alpha^2 K} \tag{4.31}$$

Substituting Eqn. (4.31) into Eqn. (4.6) yields $\xi = 0$, which implies instability. Hence, when d_4 and d_6 are simultaneously zero, the system is not stable. Following the similar arguments as in the null impedance case, it can be proven that $(d_4 \geq 0 \wedge d_6 > 0) \vee (d_4 > 0 \wedge d_6 \geq 0) \implies \xi > 0$; hence, the conditions in Eqn. (4.27) or Eqn. (4.28) hold. \square

Now let us analyse the case when $\beta + \alpha K < 0$ for completeness. In this case, Eqn. (4.24) modifies to

$$K_d \geq K \frac{\beta}{\beta + \alpha K} > 0 \quad (4.32)$$

Here, Eqn. (4.32) introduces a lower bound on the renderable stiffness. In other words, following inequalities must be satisfied to ensure $d_4 \geq 0 \wedge d_6 \geq 0$.

$$K \frac{\beta}{\beta + \alpha K} \leq K_d \leq K \frac{\eta + P_m + b}{\eta} \quad (4.33)$$

However, considering Eqns. (4.30) and (4.6), K_d values in this range will result in $\xi \leq 0$ which implies instability.

Remark 4.2.

- While deriving the passivity conditions, positive controller gains are considered, since negative gains are hardly used in practice and make the analysis much harder to follow.
- It should be pointed out that the integral gains I_m and I_t may assume zero values. A naive interpretation of Proposition 2 might lead to a misconception that passivity is lost when no velocity integral gain is employed (i.e., $I_m = 0$), since there will always be some damping b present in the plant. However, since these conditions are derived for positive control gains, the analysis needs

to be extended to include zero gains. In particular, each integrator increases the degree of the system by one. In the case of null impedance, when no integrators are employed (i.e., $I_m = I_t = 0$), the output impedance is a second order system that is unconditionally passive.

- In the case of a pure spring, when $I_m = 0$, the system cannot passively render a virtual spring of any stiffness. This is surprising in that usually integrators are known to jeopardize passivity, but in this case, a minimum amount of integral gain is necessary to render an impedance passively. When only $I_t = 0$, Proposition 3 remains valid.
- Note that null impedance is mathematically equivalent to zero virtual stiffness. Consequently, if K_d is set to zero, Proposition 3 reduces to Proposition 2.
- Table 4.1 reports the necessary and sufficient conditions for ensuring passivity when null impedance is rendered with only one integral gain. Note that, the direct dependence on b for passivity vanishes in these cases.

TABLE 4.1: The necessary and sufficient conditions for passivity when one integrator gain is set to zero

$$\frac{I_m = 0}{I_t = 0} \left| \begin{array}{l} J < J_{max}^{null}|_{I_m=0} \\ J \leq J_{max}^{null}|_{I_t=0} \end{array} \right.$$

4.3 Discussion

In this chapter, we have rigorously derived the necessary and sufficient conditions to passively render two widely adopted impedance models of zero impedance and pure stiffness under the prominent cascaded velocity-force control architecture. These results provide the least conservative bounds for all positive controller gains.

In particular, Tables 4.2 and 4.3 report the passivity bounds for the system model in Figure 1 for rendering a null impedance and a virtual spring, respectively. The notations used in [54, 60, 61] are mapped to ours to enable easier comparisons. Note that results provided in [54, 60, 61] are sufficient, but not necessary conditions. In particular, the bounds reported in [60, 61] are quite conservative. While the bounds provided in [54] relax the previously established passivity constraints [60, 61], these bounds still remain conservative.

The difference between the conditions reported in [54] and our results are relatively small for null impedance rendering case, while it becomes more pronounced for pure spring rendering case. In particular, for null impedance rendering case, the bound on inertia is relaxed by a factor of $(1 + 1/(P_m I_t))$, while the bound on b stays the same. However, the necessity of the bound on b was proven for the first time in the present work. This allowed us to remark the unexpected adversary effect of physical

TABLE 4.2: Design Guidelines for Rendering Null Impedance

Vallery <i>et al.</i> [60, 61]	$P_m > J \wedge P_m > 2I_m \wedge P_t > 2I_t$
Accoto <i>et al.</i> [54]	$J < \frac{(P_m+b)(P_m P_t)}{P_m I_t + P_t I_m} \wedge b < \frac{P_t I_m}{I_t}$
Ours	$J < \frac{(P_m+b)(1+P_m P_t)}{P_m I_t + P_t I_m} \wedge b < \frac{P_t I_m}{I_t}$

TABLE 4.3: Design Guidelines for Rendering Virtual Spring

Vallery <i>et al.</i> [60, 61]	$P_m > J \wedge P_m > 2I_m \wedge P_t > 2I_t \wedge K_d < K_d^{max} _{b=0}$
Accoto <i>et al.</i> [54]	$J < \frac{(P_m+b)(P_m P_t)}{P_m I_t + P_t I_m} \wedge b < \frac{P_t I_m}{I_t} \wedge K_d < K_d^{max}$
Ours	$J < \frac{(P_m+b)(\Delta K P_m P_t + K)}{\Delta K (P_m I_t + P_t I_m)} \wedge b < \frac{P_t I_m}{I_t} \wedge K_d < K_d^{max}$ (Eqn. (4.26))

damping on system passivity, as it unintuitively implies that too much dissipation may violate passivity.

For the spring rendering case, the bound on J is relaxed by a factor of $1+(K/(P_m P_t \Delta K))$, where $\Delta K \triangleq K - K_d$. Hence, the smaller ΔK (i.e., the stiffer virtual spring rendered), the less strict the bound on J becomes. Finally, the bound on K_d and b remain the same as it has been reported in the literature [54]. Note that the presence of damping not only imposes an additional passivity constraint but also reduces the K-width of the system (i.e., K_d^{max}). This has been reported through an inequality plot that shows the inverse relationship between the actuator damping b and the normalized maximum renderable stiffness K_d^{max}/K [54].

To maximize the K-width of the system, the velocity integral gain I_m needs to be maximized. Our least conservative bounds allow I_m to attain its maximum value without violating passivity; thus, enlarge the K-width of the system to its theoretical limit.

Another important finding of this study reveals that the presence of damping necessitates an extra passivity constraint. If the actuator is modeled as pure inertia, that is, $b = 0$, the condition in Proposition 2 reduces to

$$J_{max}^{null} < \frac{P_m(1 + P_m P_t)}{P_m I_t + P_t I_m} \quad (4.34)$$

Hence, when physical damping is neglected in the system model such that the actuator is modeled as pure inertia, a necessary condition for passivity is missed. This result is counterintuitive in that increasing damping is typically expected to result in less conservative passivity conditions due to its dissipative nature. However, this intuition fails in the presence of integral controllers and introduction of physical actuator damping into the system model imposes an additional constraint to ensure passivity, instead of relaxing passivity conditions. Therefore, physical damping should not be neglected in the passivity analysis, especially if integrators are utilized. This result surprisingly demonstrates the adversary effect of physical damping on passivity.

To emphasize this fact, a numerical example is provided. Assume we have the SEA plant as given in Table 5.1. Two controllers are suggested: The first controller has been tuned according to Proposition 2, while the second controller has been tuned according to Eqn. (4.34). The numerical values for the control parameters used in the simulation are reported in Table 4.4. In Chapter V, we show that larger I_t gains provide better rendering performance for null impedance. Hence, the largest possible values of I_t with a small safety margin have been chosen for both systems. Note that when the damping is included in the actuator model, the upper bound for I_t dramatically decreases because of the additional constraint introduced due to the presence of damping.

Figure 4.2 presents the Bode plots of these two systems. Note that, both systems are theoretically passive according to their respective actuator models that are with

TABLE 4.4

Control Gain	First Controller	Second Controller
P_m	20 Nm s/rad	20 Nm s/rad
P_t	5 rad/(s Nm)	5 rad/(s Nm)
I_m	10 Nm/rad	10 Nm/rad
I_t	15 rad/(s ² Nm)	80 rad/(s ² Nm)

and without damping. However, to test the controllers, damping is included in the simulated actuator model of both systems, since some level of dissipation is always present in physical systems.

Clearly, the second controller outperforms the first one, but at the expense of passivity. Simulation results indicate that the phase of the second controller passes 90° for a range of low frequencies and goes up to 93.5° . This result serves as a counter-example for the commonly employed assumption that neglecting damping results in more conservative passivity conditions.

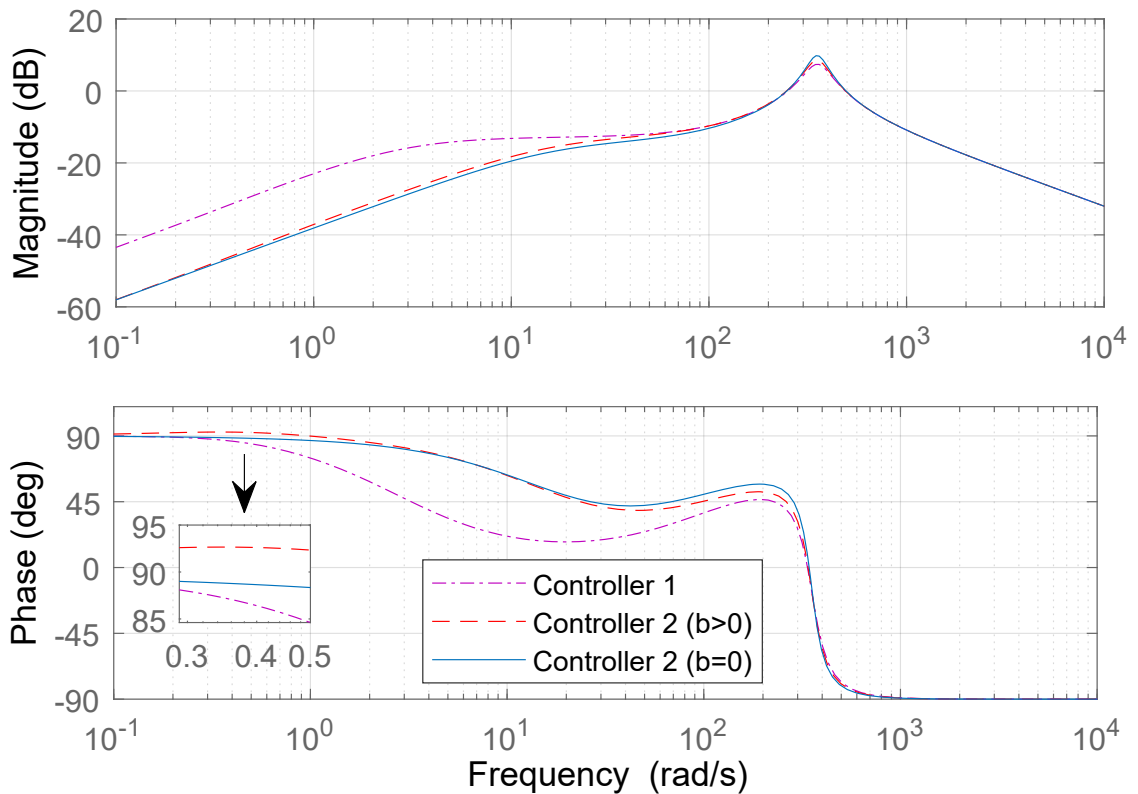


FIGURE 4.2: The effect of actuator damping on system passivity

In fact, similar counter-examples that falsify the presumption that an addition of damping relaxes the passivity bounds have also been noted in the literature. In particular, a numerical parameter space search was used in [17] to analyse the passivity of Natural Admittance Control [38] and an adversary relationship between the

integral control gain and the virtual damping parameters in the presence of physical damping has been noted. Similarly, in [65], the need for verifying passivity at the upper and lower bounds on the damping parameter has been advocated within the concept of bounded impedance passivity. Our results are in good agreement with these earlier observations and rigorously support them by proving the necessity of bounds on integral gains when physical damping of the system is included in the system model.

Chapter 5

Analysis of Rendering Fidelity

In this chapter, the effect of the controller gains on the system response is analyzed through a systematic set of simulations. Visualization of passivity through Bode plots is convenient since the passivity of linear one-port systems is strictly a phase condition. More precisely, the phase of the system is restricted to the interval $[-90^\circ, 90^\circ]$ at all frequencies.

Since PI controllers are employed for both the inner velocity and the outer torque control loops, there are four controller parameters to choose namely, $P_m, P_t, I_m,$ and I_t . Firstly, Bode plots are drawn with respect to the changes in a certain controller gain, (e.g., P_m) while keeping the other three gains constant to analyze the effect of each individual parameter on the system behaviour. Next, design guidelines are outlined to choose the controller gains that render the system passive, while exhibiting good performance for haptic impedance rendering. The realistic values for the SEA plant parameters used in all simulations are reported in Table 5.1.

TABLE 5.1: Physical parameters considered for the SEA plant

Mechanical Parameters of SEA	
J	$0.2 \text{ Nm}/(s^2\text{rad})$
b	$3 \text{ Nms}/\text{rad}$
K	$250 \text{ Nm}/\text{rad}$

5.1 Effects of Controller Gains on Null Impedance Rendering

In this section, we analyze the effect of each controller gain in the case of null impedance rendering. For each simulation, we start with a base case scenario with certain controller gains reported in Table 5.2. Then, we increase each gain individually to see its effect on the system response through Bode plots.

It is observed that the system behaviour may be grouped into three phases. In the first phase, where the input frequency has a low value, the system displays the characteristics of a pure inertia. In the second phase, where the input frequency has an intermediate value, viscous damping behaviour is observed. In the third phase, where the input frequency has a high value, the system response reduces to that of the physical spring employed in the SEA plant. As argued earlier, this is due to the fact that the compliance between the actuator and the load acts as a physical filter against high-frequency force components, which provides safety and robustness against unexpected collisions and impacts.

Figure 5.1 shows the effect of the velocity proportional gain P_m on the system response. Plots are constructed with different controller gains of P_m , and the legend indicates the gain values used during the simulation. The frequency response of the physical spring employed in the SEA (labeled as K) was also included in the plots to show that at higher frequencies the system response converges to that of the physical spring.

TABLE 5.2: Nominal controller gains to render null impedance

Controller Gains	
P_m	20 Nm s/rad
P_t	5 rad/(s Nm)
I_m	10 Nm/rad
I_t	5 rad/(s ² Nm)

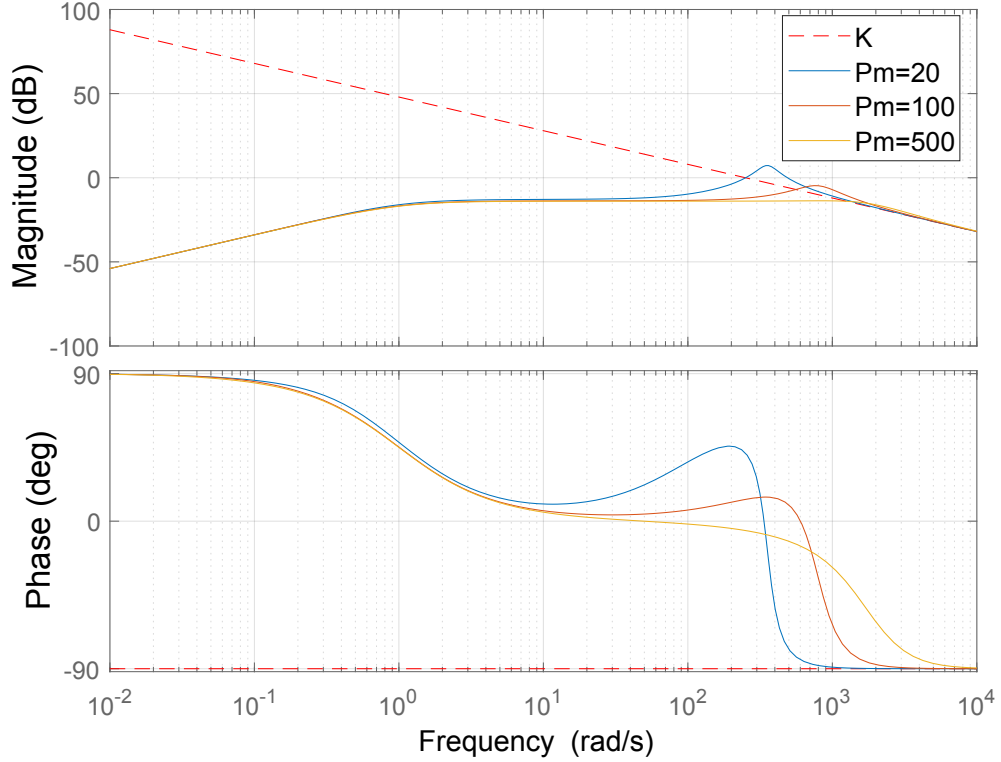


FIGURE 5.1: Null impedance rendering with various velocity proportional gains

Plots indicate that P_m has no significant effect in the first phase (i.e., the inertial zone), but it helps to smooth out the transition from the second phase to the third phase by decreasing the resonant peak at the corresponding cut-off frequency. Theoretically, there exists no upper bound on P_m that violates passivity. However, a practical bound is likely to be imposed by physical bandwidth limitation of the actuator.

Figure 5.2 shows the effect of the velocity integral gain I_m . Plots indicate that I_m has a negligible effect on the overall system response. On the other hand, increasing I_m is useful to preserve passivity against the actuator damping bound (i.e., b_{max}), but too much increase may jeopardize passivity by violating the actuator inertia bound (i.e., J_{max}), as can be seen from Proposition 2.

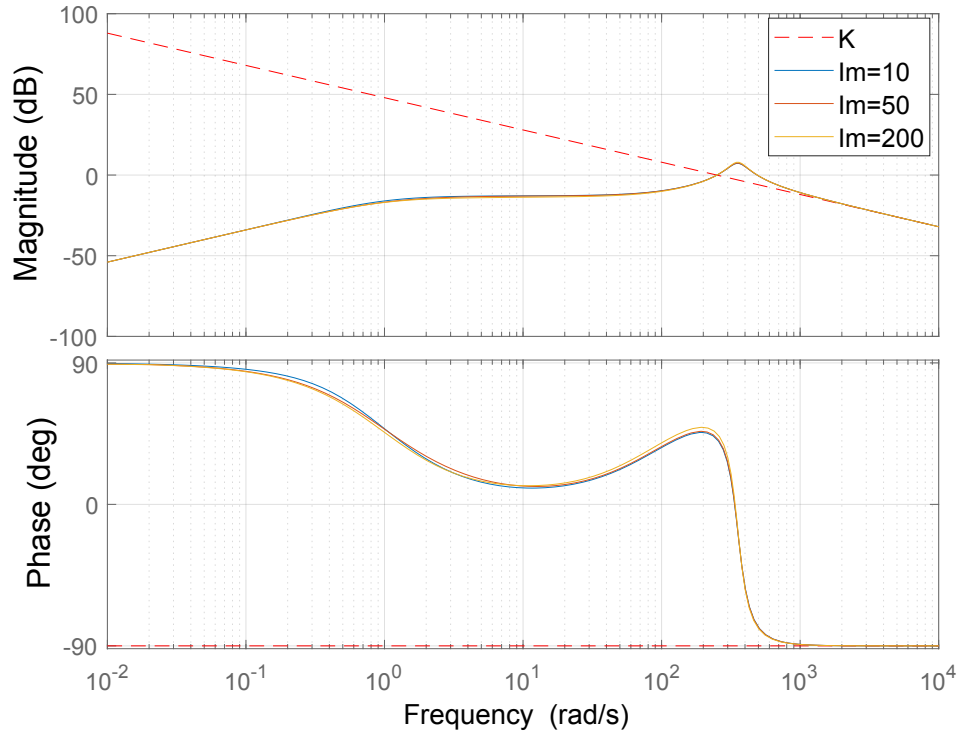


FIGURE 5.2: Null impedance rendering with various velocity integral gains (I_m)

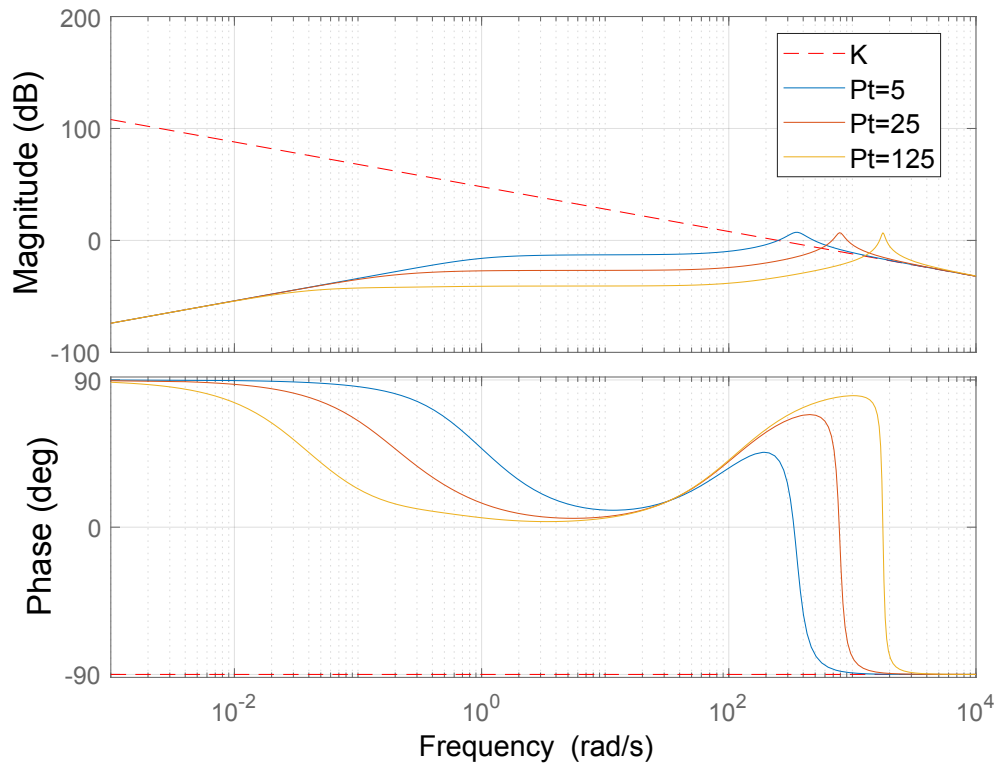


FIGURE 5.3: Null impedance rendering with various torque proportional gains P_t

Figure 5.3 shows the effect of the torque proportional gain P_t . Plots indicate that larger values of P_t shrink the inertial zone, which may not be favorable. On the other hand, since the system reaches the damping zone earlier, the apparent impedance stays lower for larger P_t , as can be inspected from the magnitude plots. Hence, the selection of P_t involves a trade-off between the control bandwidth and transparency performance. If the operating frequency of the application is low, then P_t may be chosen high.

Figure 5.4 shows the effect of the torque integral gain I_t . Plots indicate that an increase in I_t dramatically improves system performance, since not only the inertial zone gets enlarged, but also the apparent inertia is lowered. However, there exists an upper bound on I_t due to the passivity conditions given in Proposition 2.

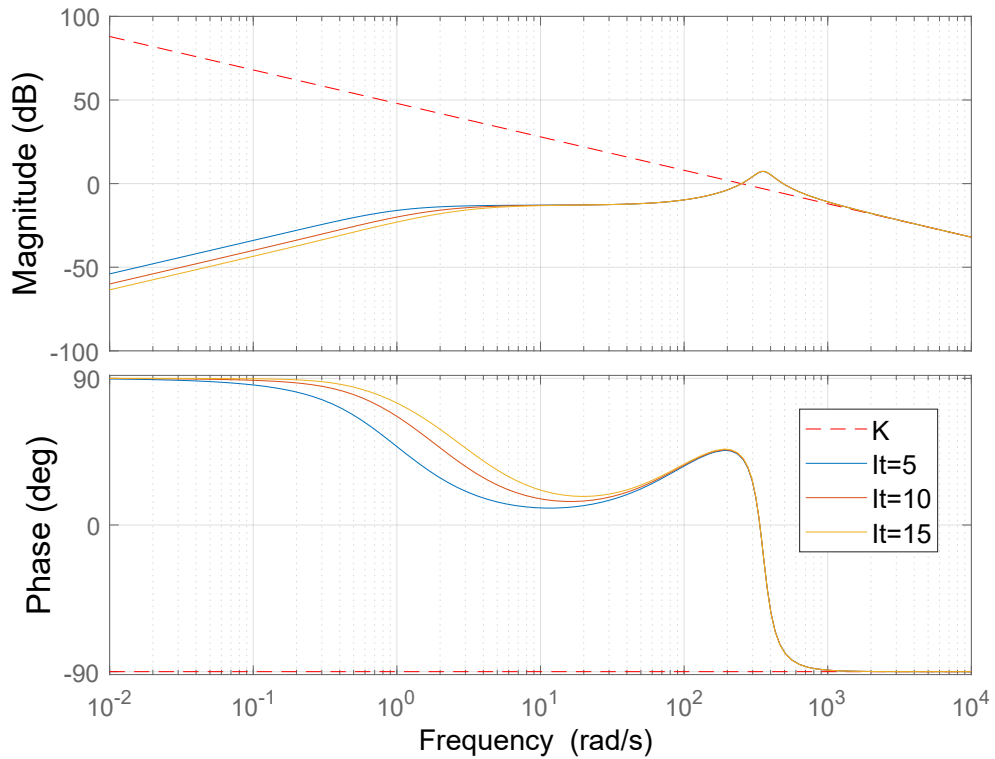


FIGURE 5.4: Null impedance rendering with various torque integral gains I_t

5.1.1 Design Guidelines for Null Impedance Rendering

The analysis shows that the outer torque controller is the main determinant of performance during null impedance rendering. Increasing I_t results in better rendering performance by reducing the apparent inertia, as well as widening the inertial zone. While the analysis indicates that the inner velocity controller does not have a significant effect on system response, in practice a fast and robust controller is still desirable to render the actuator as an ideal motion generator under unmodelled parasitic forces.

As I_t gets larger, which is desired for better performance, passivity is at stake as can be seen from Eqn. (4.15). Hence, relatively aggressive gain values for P_m and I_m are recommended to design a robust inner motion controller, as well as to preserve passivity without sacrificing good null impedance rendering performance.

5.2 Effects of Controller Gains on Pure Stiffness Rendering

In this section, we analyze the effect of each controller gain while rendering a virtual spring, using a similar approach as in Section 5.1.

Once again, it is observed that the overall behaviour of the system may be grouped into three phases. In the first phase, the virtual stiffness of the desired value is successfully displayed. In the second phase, damping behaviour is observed. In the third phase, as expected, the system behaviour reduces to that of the physical spring employed in the SEA. The numerical values for system parameters used in simulations are reported in Table 5.3.

TABLE 5.3: Nominal controller gains to render a pure spring

System parameters	
P_m	20 Nm s/rad
P_t	30 rad/(s Nm)
I_m	100 Nm/rad
I_t	5 rad/(s ² Nm)
K_d	50 Nm/rad

Figure 5.5 shows the effect of the velocity proportional gain P_m . Plots indicate that P_m does not have a significant effect in the first phase, but high values of P_m lower the resonant peaks that occur at the phase transitions. Theoretically, there exists no upper bound on P_m that causes violation of passivity.

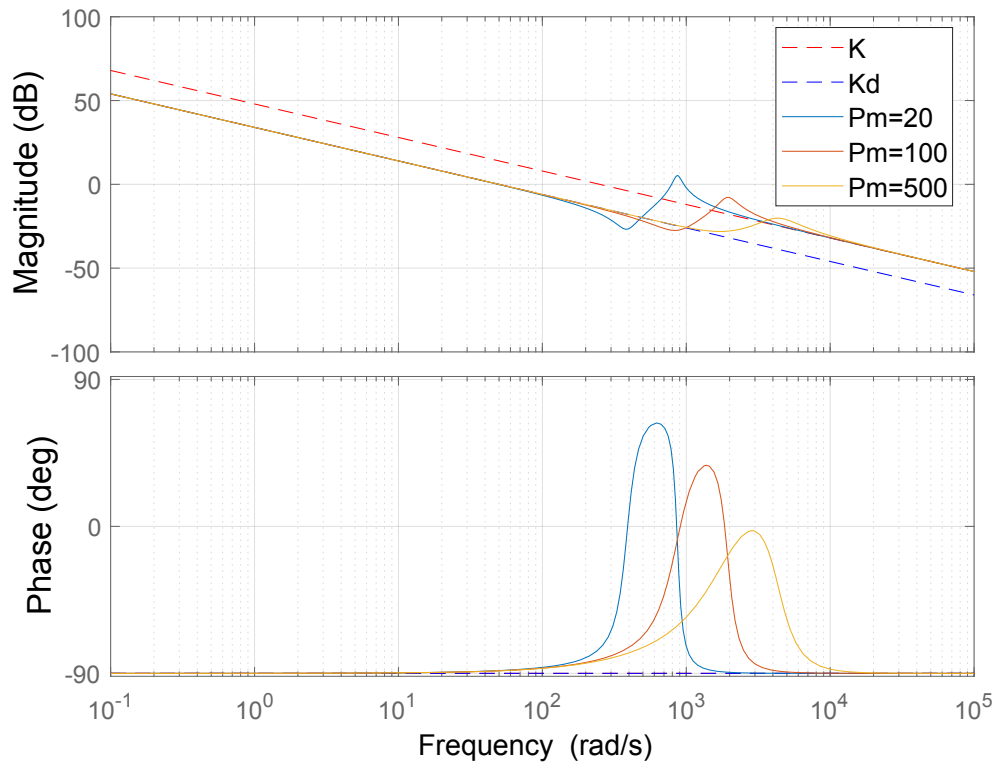


FIGURE 5.5: Pure spring rendering with various velocity proportional gains P_m

Figure 5.6 shows the effect of the velocity integral gain I_m . Plots indicate that I_m does not have a significant effect on the overall system response. However, it is the

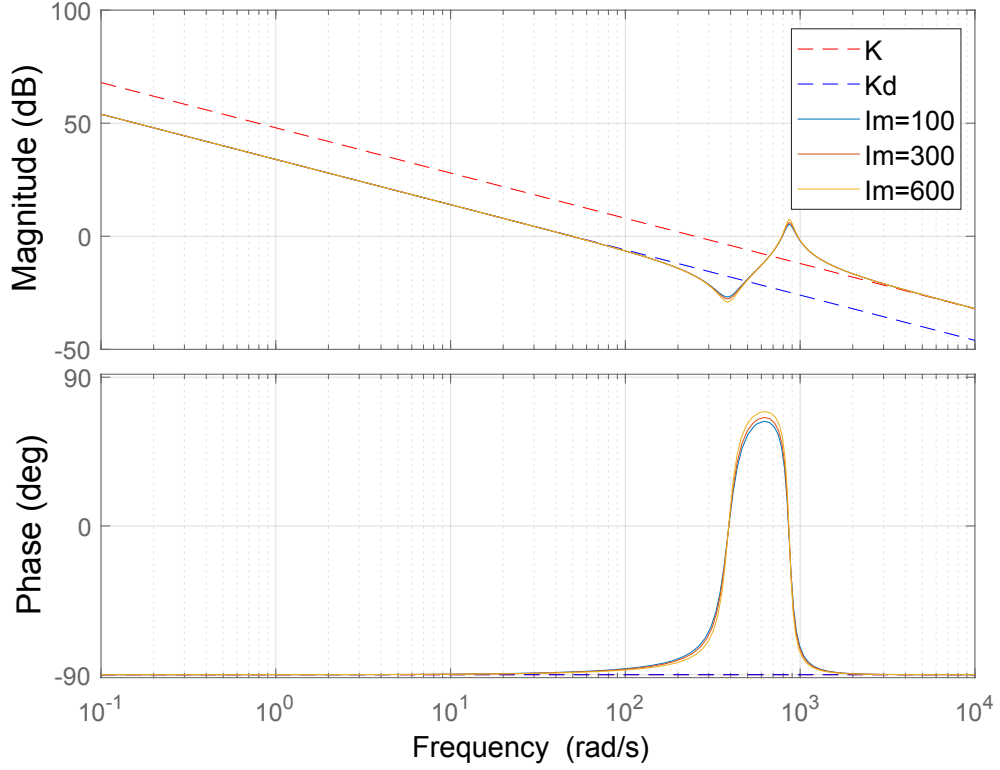


FIGURE 5.6: Pure spring rendering with various velocity integral gains I_m

most critical parameter to determine the maximum renderable stiffness $K_{d_{max}}$. It can be seen from Eqn. (4.26) that $K_{d_{max}} \rightarrow K$ as $I_m \rightarrow \infty$. For any other controller gain, this limit goes to a value less than the physical stiffness K of SEA.

Figure 5.7 shows the effect of the torque proportional gain P_t . Plots indicate that increasing P_t provides better performance, since the desired stiffness is successfully rendered for a wider frequency range. However, on the downside, it also increases the resonant peaks at the phase transitions.

Figure 5.8 shows the effect of the torque integral gain I_t . Plots indicate that it does not significantly affect the system response. Moreover, large values of I_t jeopardize passivity, as can be seen from Proposition 3. If I_t is set to zero, the value of I_m must be set to $I_m \geq KK_d/\Delta K$, in order to be able to display desired stiffness K_d , as can be seen from Eqn. (4.24). Along these lines, while it is theoretically alluring to set I_t to zero, while a small I_t may be preferred in practical implementations to eliminate steady-state errors.

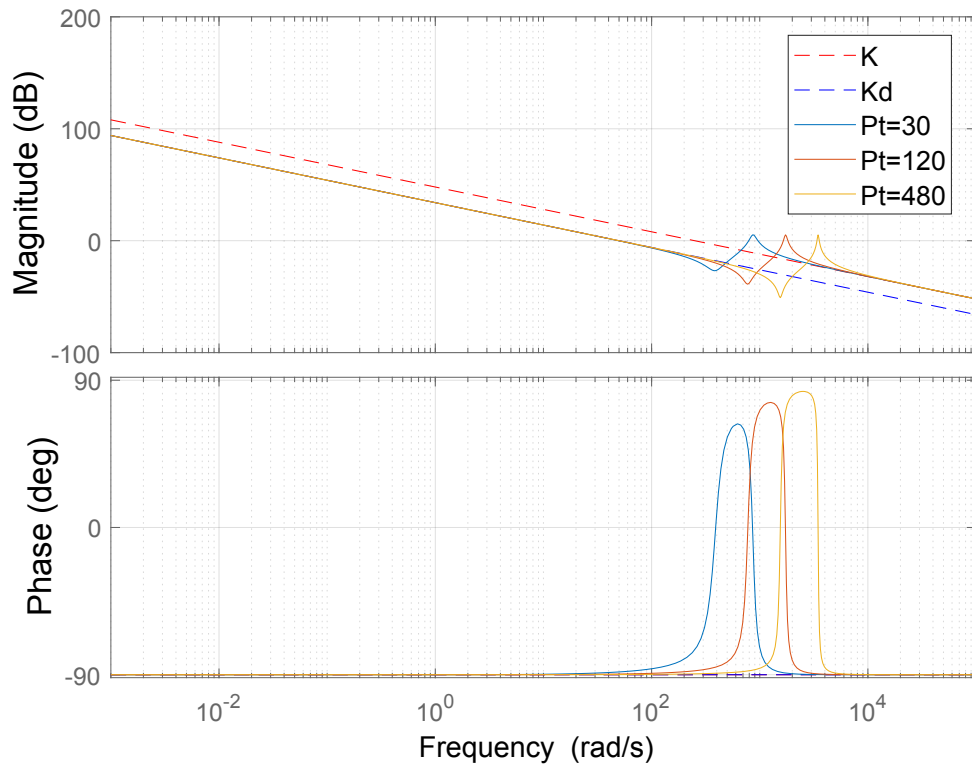


FIGURE 5.7: Virtual spring rendering with various torque proportional gains P_t

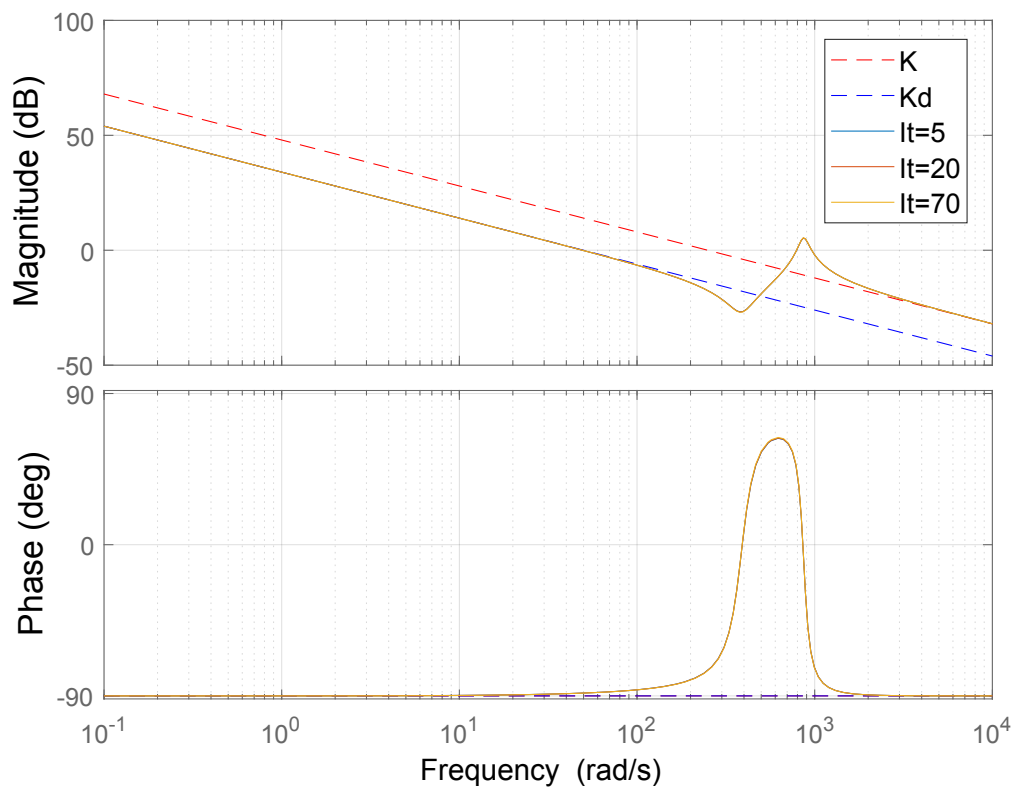


FIGURE 5.8: Virtual spring rendering with various torque integral gains I_t

5.2.1 Design Guidelines for Pure Stiffness Rendering

The analysis indicates that P_t is the main determinant of the performance during pure stiffness rendering, since the frequency up to which the desired stiffness is successfully displayed is directly related to P_t . On the other hand, a sufficiently large value of I_m must be employed to ensure that desired stiffness can be passively rendered. Hence, I_m plays a crucial role in determining the K-width of the system.

A high value of P_m is also preferred as it smoothens the transitions between phases. Furthermore, an increase in P_m helps to preserve passivity according to Proposition 3.

I_t does not have a significant effect on rendering performance. Moreover, it has an adverse effect on preserving passivity. A small value of I_t may be injected into the system to eliminate the steady state errors due to constant disturbances, such as parasitic forces due to stiction. Pure P control may be applied at the outer torque controller, if the system does not suffer from undesirable steady-state response.

5.3 Overall Design Guidelines

Many applications in pHRI require frequent switching between active backdrivability (null impedance rendering) and virtual fixtures (pure spring rendering), such as haptic virtual environments that contain a unilateral constraint [58]. Hence, it is desirable to determine a single set of controller gains that ensures passivity for both impedance models. Fortunately, the passivity bounds on controller gains for both impedances are not in conflict. Hence, to design a passive controller that performs well for both impedances, the bounds provided in Proposition 2 and 3 can be used to adjust the controller gains sufficiently high to meet the specifications of the application without jeopardizing passivity. More precisely, we must set relatively high gains for the inner loop to make it an ideal motion source that rejects interaction disturbances effectively. Note that, robust velocity control requires orders of magnitude high integral gain as it corresponds to proportional gain in position level. Hence, it is a good practice to start with tuning the inner loop gains to get an adequate velocity controller.

Chapter 6

Experimental Validation

This chapter presents the experimental verification of the impedance control of velocity sourced SEA. The experimental setup utilized is an SEA brake pedal proposed in [10]. Figure 6.1 depicts this mechanical design. Leaf springs are arranged to form a compliant cross-flexure joint. The deflection of the springs is measured by a linear encoder for force estimation. Hall effect sensors on the rotor provides high fidelity motor velocity measurements. The SEA device is controlled in real-time with a sampling rate of 1000 Hz. The inner motion control loop is implemented in the hardware of the motor drivers and runs at 10 kHz.

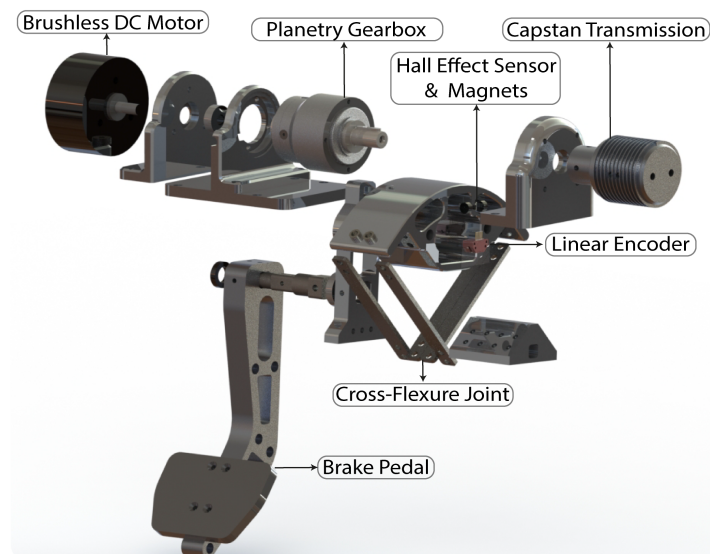


FIGURE 6.1: Experimental setup: SEA brake pedal

6.1 System Identification

We have derived non-conservative passive controller design guidelines in Chapter 4. We have shown that the actuator inertia and damping, as well as the compliance of the spring limit the control gains to obey passivity. Proper selection of control gains necessitates the identification of the physical system parameters. While the inertia of the actuator and the compliance of the spring may be derived from the first principles, system identification must be performed to estimate the effective damping of the system.

We have performed closed-loop system identification for the system containing the inner motion loop whose block diagram is depicted in Figure 6.2. It is white box modelling since we fully know the structure of the controlled plant. We only need to determine the numerical values of J and b parameters. The motion controller gains P_m and I_m are tuned to meet the performance criteria for robust motion control; hence predetermined. The physical spring torque τ_s acts a disturbance to the system. However, it is safe to neglect it since the motion controller is tuned to reject these disturbance forces robustly. Furthermore, the feedforward compensation of this interaction force is common in control of SEAs. Along these lines, no exogenous input is applied to induce the spring deflections. Under these modeling assumptions, the transfer function from the commanded velocity to measured velocity reads as

$$\frac{\omega_m}{\omega_d} = \frac{P_m s + I_m}{J s^2 + (P_m + b)s + I_m} \quad (6.1)$$

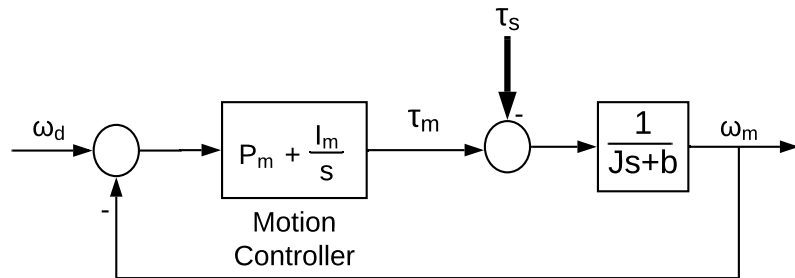


FIGURE 6.2: Closed loop motion controlled system

We excite the system using two different chirp signals with frequencies ranging up to 10 Hz and 5 Hz, respectively. We use the first excitation signal for estimation and the second one for validation. We utilize Matlab's *System Identification Toolbox*[®] to fit an LTI model to the experimental data. In particular, a transfer function with 1 zero and 2 poles is fit by fixing the position of the zero to $P_m/I_m = 0.0167$ thanks to our prior knowledge of the motion controller gains. The estimated closed-loop transfer function reads as

$$T_{CL}(s) = \frac{0.0841s + 5.036}{0.0033s^2 + 0.2503s + 5.036} \quad (6.2)$$

The goodness of fit is 95% in terms of the normalized root mean square error (NRMSE). This model together with the experimental data are plotted in Figure 6.3.

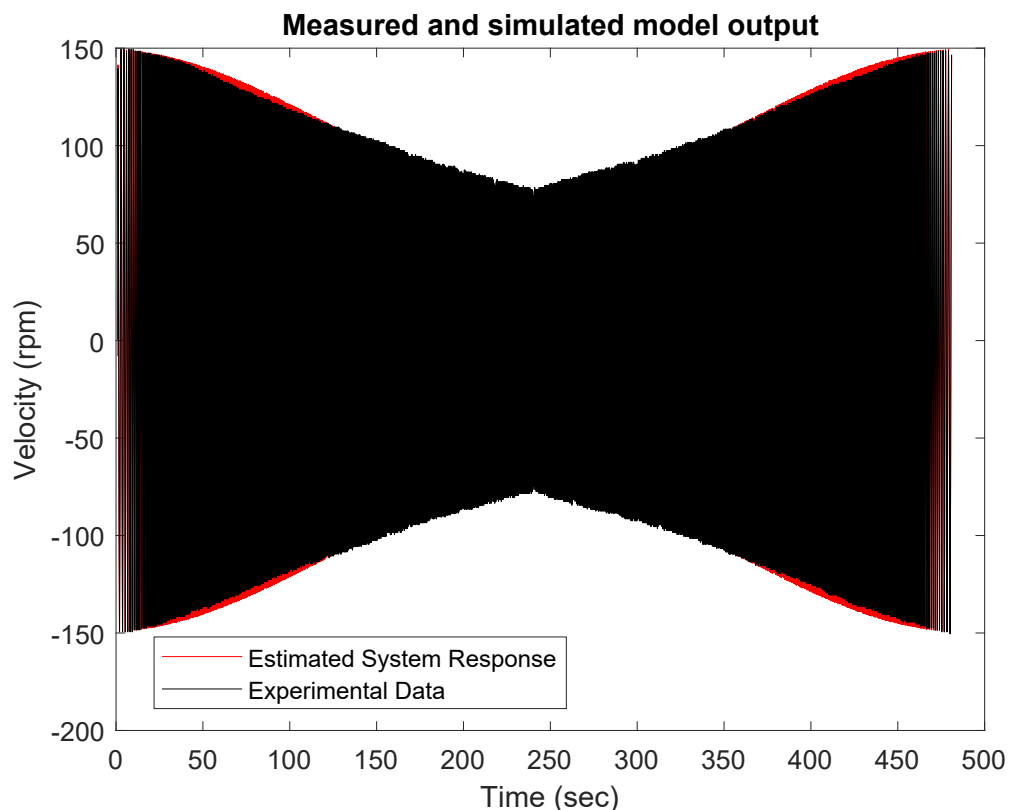


FIGURE 6.3: Experimental and simulated model output during system identification

The main advantage of the velocity-force cascade control of SEA lies on the idea of robust inner motion loop to effectively attenuate disturbances and suppress the actuator dynamics in low frequencies. In fact, as seen in Figure 6.4, the closed-loop transfer function of motion controlled SEA can be modeled as a first order low pass filter. This approximation is especially valid for frequencies below the actuator bandwidth.

Figure 6.4 reports the Bode plots of the closed-loop identified system in Eqn. (6.2) and a reduced model which is evaluated as $T_{CL}(s) = 30/(s + 30)$. Clearly, first order ideal low-pass filter model of the closed-loop motion controlled system is a valid approximation within the bandwidth of the system.

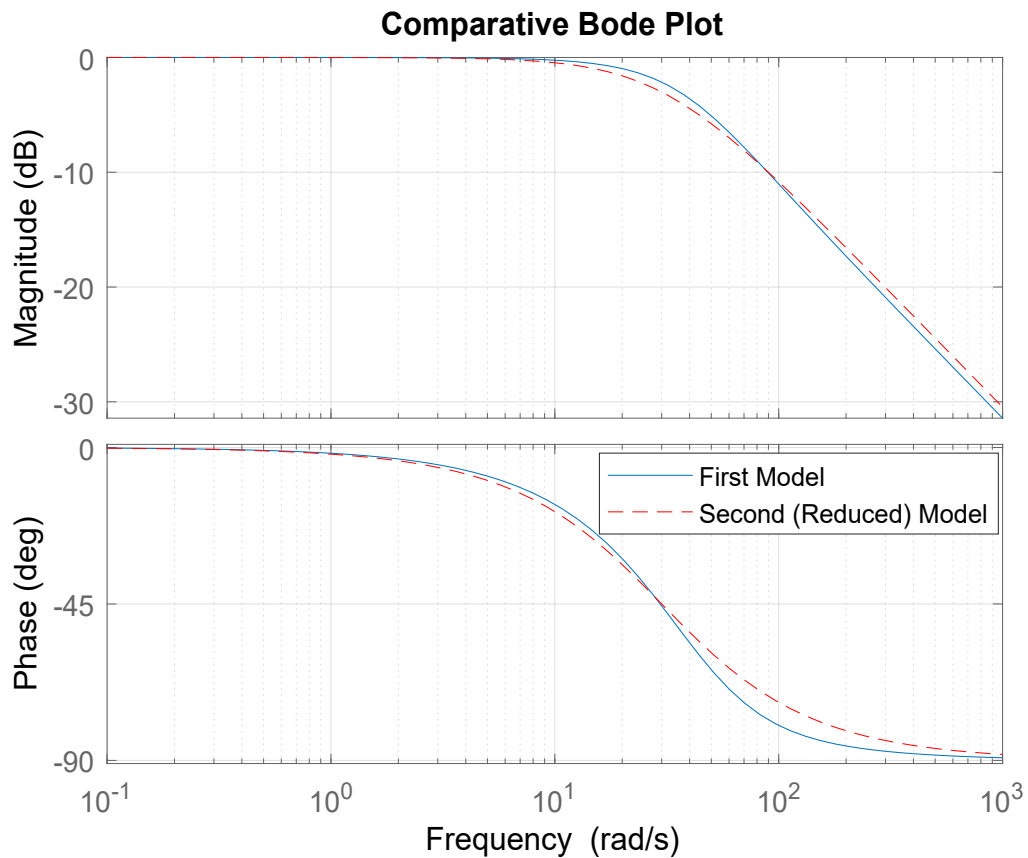


FIGURE 6.4: Comparative bode plot of the real and reduced model

Thanks to this model reduction, simpler passivity analysis becomes viable. However, the conditions we have derived in Chapter 4 are more generic, since they also account for the actuator inertia and damping.

Until now, we have discussed the procedure of characterizing the actuator dynamics. The characterization of the spring compliance is straightforward. In particular, we applied static torques by putting known weights on the load side of the SEA and measured the corresponding deflections. Table 6.1. reports the experimentally identified plant parameters.

TABLE 6.1: Identified parameters of the SEA brake pedal

Description	Symbol	Value
Inertia of the actuator	J	$0.0033 \text{ Nm}/(s^2\text{rad})$
Damping of the actuator	b	0.1662 Nm.s/rad
Stiffness of the complaint element	K	360 Nm/rad

6.2 Torque Controller Tuning

This section presents the experimental procedure used to tune the force/torque controller employed in a velocity-sourced SEA. Note that, we have already tuned the inner motion controller gains during closed-loop system identification. Impedance control requires an accurate force controller. Thereby, it is required to tune the outer torque control gains to meet the performance criteria without violating passivity. Table 6.2 reports the control gains used throughout the experiments. They are valid for the rest of the chapter unless otherwise stated.

TABLE 6.2: Control parameters of the SEA plant for haptic impedance rendering

Description	Symbol	Value
Proportional velocity gain	P_m	0.5 Nm/rad
Integral velocity gain	I_m	50.35 Nm.s/rad
Proportional torque gain	P_t	0.1 rad/(sNm)
Integral torque gain	I_t	$0.05 \text{ rad/(s}^2\text{Nm)}$

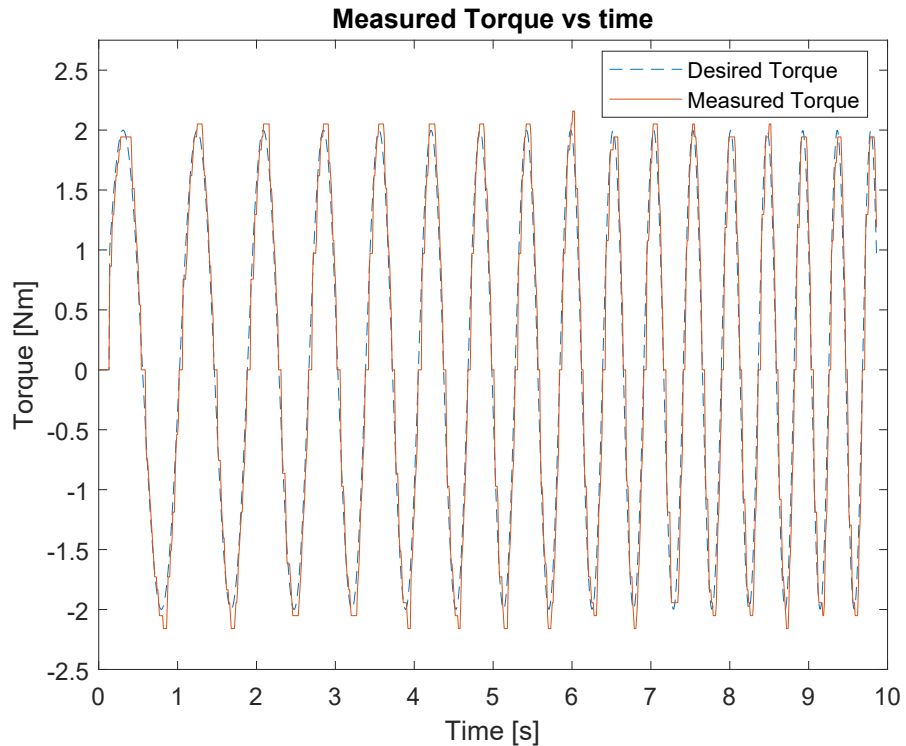


FIGURE 6.5: Chirp tracking reference tracking performance for a frequency range up to 4Hz

Figure 6.5 reports the torque tracking performance of the SEA plant for a chirp reference signal up to 4 Hz with 2 Nm peak-to-peak amplitude. The normalized MRS error for this experiment stays under 5 %.

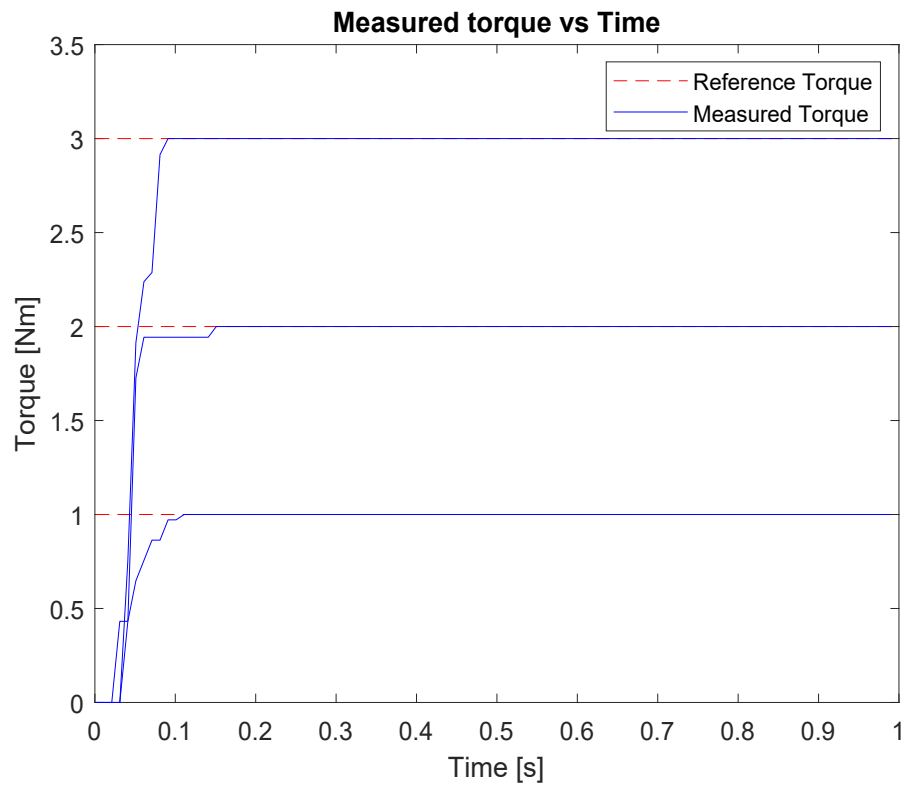


FIGURE 6.6: Set-point torque tracking reference tracking performance for 1 Nm, 2 Nm and 3 Nm

Figure 6.6 reports the control performance to a set of set-point reference torque values of 1 Nm, 2 Nm and 3 Nm. The steady state error is practically zero. The rise time is less than 100 ms. The settling time is less than 200 ms. Thus, we use the control gains summarized in Table 6.2 for the rest of experiments.

6.3 Impedance Rendering Performance

This section presents the performance evaluation of the device for haptic impedance rendering. Pure springs and null impedance are displayed. These two simple linear models serve as the basic building blocks for a large variety of virtual environments.

6.3.1 Pure Spring Rendering

Two virtual springs were displayed with stiffness values of 20 Nm/rad and 40 Nm/rad for evaluation. We applied static torques with known values on the end-effector and measured the corresponding rotor displacements. Figure 6.7 reports the torque-deflection data from these measurements. Best linear fits agree with the commanded stiffness values with less than 0.05% NMRSE.

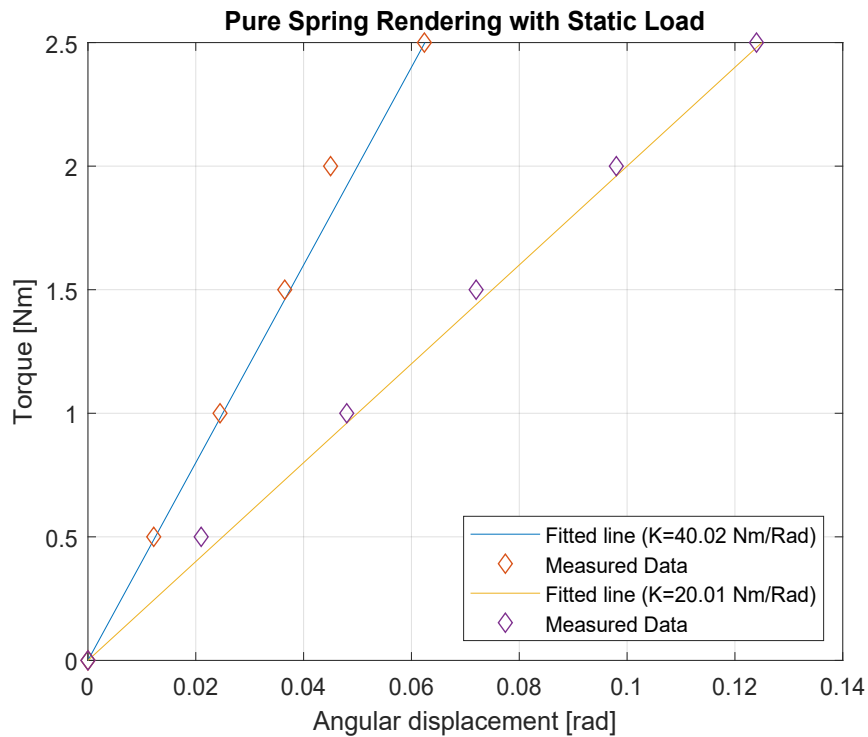


FIGURE 6.7: Experimental verification of rendering two virtual torsional springs with 20 Nm/rad and 40 Nm/rad stiffness

The SEA device is designed to interact with humans. Thereby, we also need to evaluate the impedance rendering performance when dynamic loads are applied to the device by the human operator. The load torques exerted by the human user are estimated through the measurements of spring deflections.

Figure 6.8 reports results from the interaction of the human subject with a relatively hard torsional virtual spring. More precisely, the virtual spring has stiffness value of 40 Nm/rad. The device safely delivers the required torques to display the desired virtual environment to the user. The desired torque reference is computed by the outermost impedance controller. NMRSE value for this experiment is reported as 3.3% where the range of the output torques is used for normalization.

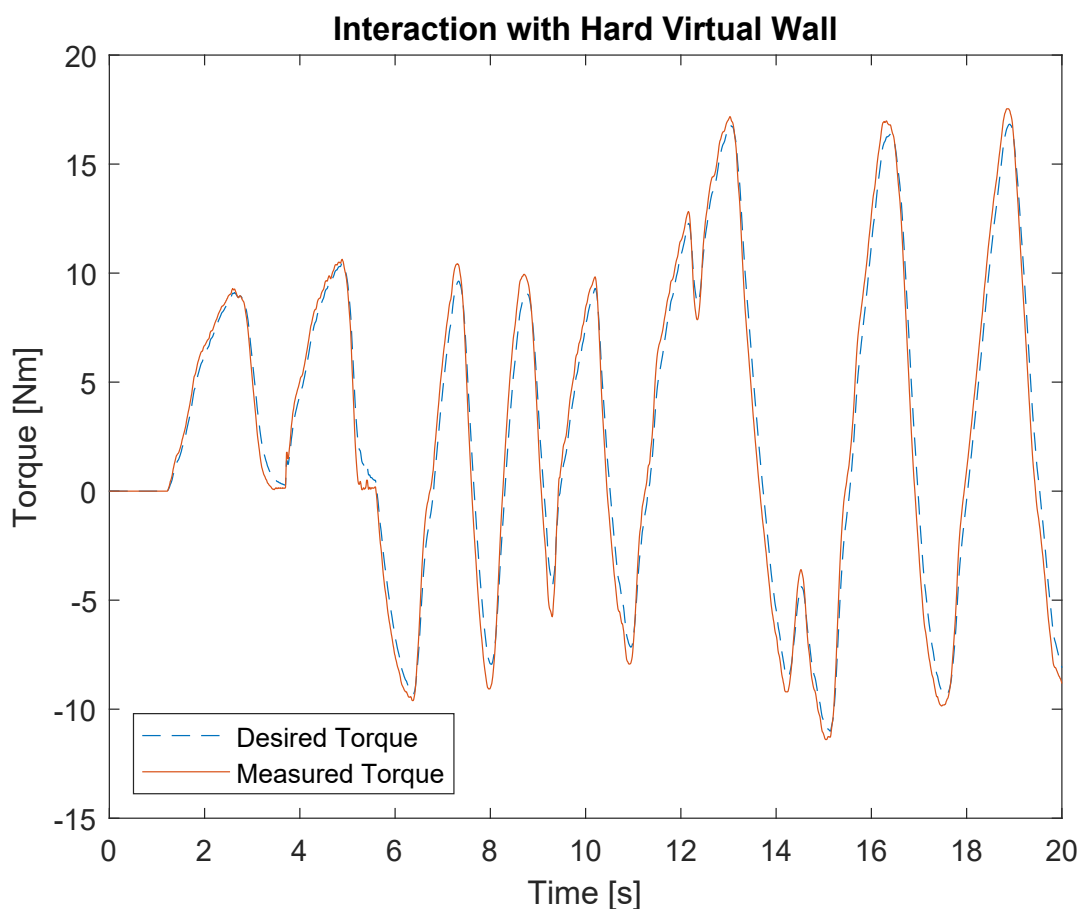


FIGURE 6.8: Human subject interacting with a hard virtual wall

Figure 6.9 reports the interaction of the human subject with a relatively soft torsional virtual spring with stiffness value of 20 Nm/rad. This time the NMRSE is reported as 5.8%. The relatively high error when rendering soft stiffness is due to the physical bandwidth limitation of inner motion loop. In particular, since the user can cause much larger deflections with softer virtual environments, the actuator cannot move fast enough to compensate for these large deflections in a timely manner.

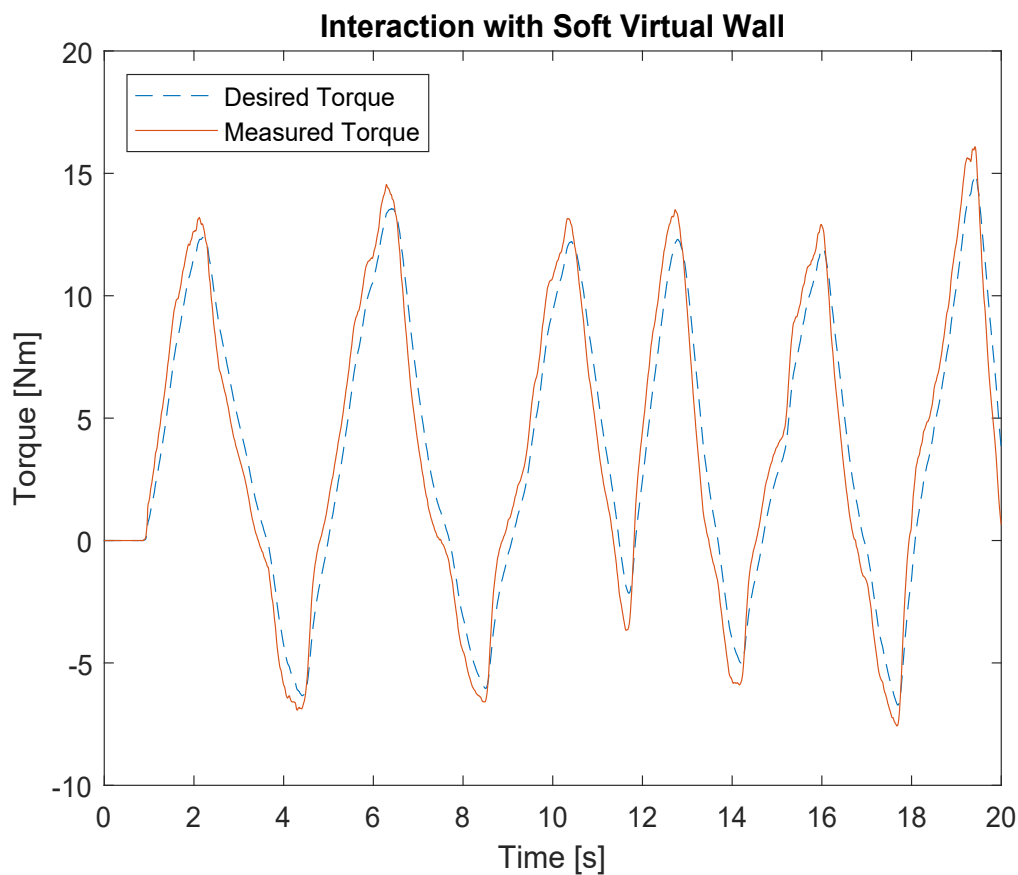


FIGURE 6.9: Human subject interacting with a soft virtual wall

6.3.2 Null Impedance Rendering

This section presents the performance evaluation of the device for displaying null impedance or equivalently, providing active backdrivability. The device is enforced

to seem transparent to the human user by minimizing the reflected output impedance of the SEA device.

We perform two sets of experiments. In the first case, the subject directly interacts with the device when it is operating at the null impedance mode. In the second case, the subject pushes the pedal with a potato chip. Figure 6.10 reports the measured output torques in these experiments. In particular, the maximum output torque is less than 1.5 Nm in magnitude when the subject directly interacts with the device and even lesser when the pedal is pushed with a chip without breaking it. Note that, faster interactions result in lower active backdrivability due to actuator bandwidth limitations. Even though ideally the output torque should be zero, 1.5 Nm is acceptable as the maximum output torque capability of the device is 40 Nm, indicating a parasitic torque of 3.75%.

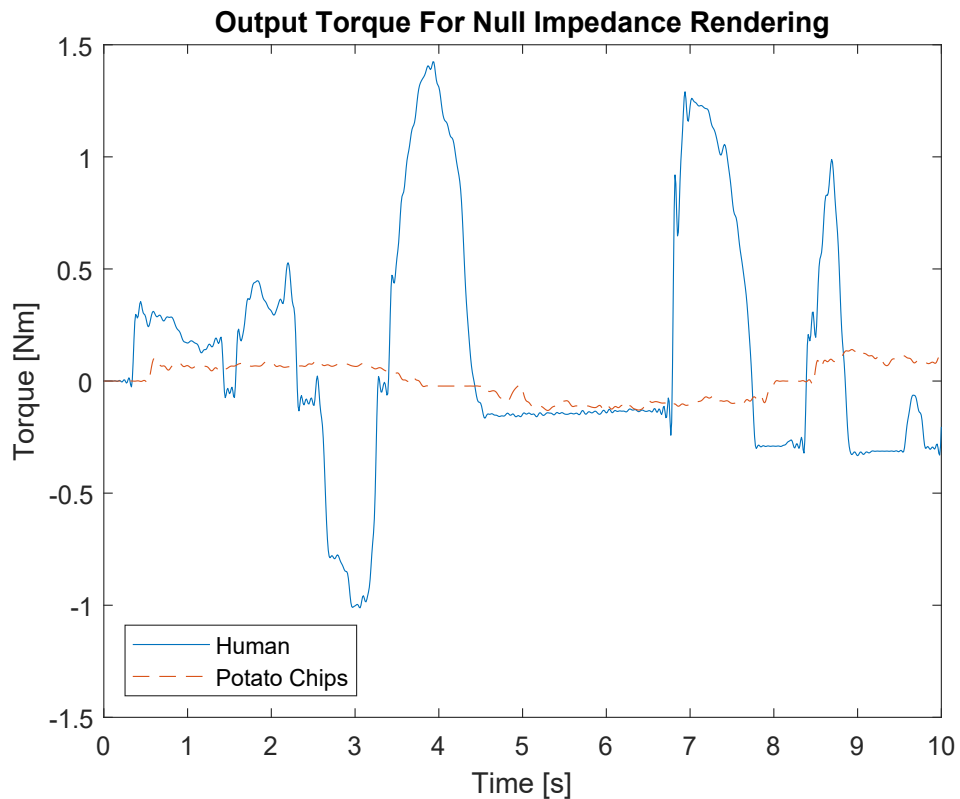


FIGURE 6.10: Human subject interacting with the device when it renders null impedance

6.4 Experimental Verification of Passivity Bounds

Experimental verification of system passivity through Bode plots might not be feasible at all times due to the challenges of experimentally obtaining the system phase. Luckily, there are alternative interpretations for passivity. In particular, a passive system must hold the coupled stability property when coupled to an arbitrary passive environment. The most destabilizing passive environments for 1-port LTI systems are pure springs and inertias as they contribute 90° phase to the system [15]. Thereby, the system passivity may be investigated by analyzing the interactions with these most destabilizing environments. Passivity is concluded if and only if there exists no set of springs or inertias that destabilize the system. This is a useful result as it is practically impossible to search for all possible passive environments with different mass-spring-damper combinations. It can be verified that pure inertia is the most destabilizing environment for SEA [53].

The coupled stability of the SEA plant when coupled to an environment with admittance $Y_e(s)$ can be analysed by applying Routh-Hurwitz criterion on the numerator of $1 + Z_{out}(s)Y_e(s)$. The environment dynamics must be expressed as an admittance due to the causality principle. The admittance of a pure inertia is expressed as $Y_e(s) = 1/J_e s$, where J_e is inertia value of the environment.

Along these lines, the characteristic equation of the coupled system that determines the stability reads as

$$\begin{aligned}
 & J J_e s^6 + J_e (P_m + b) s^5 + (I_m J_e + J K + J_e K + J_e K P_m P_t) s^4 + \\
 & (K b + K P_m + I_t J_e K P_m + I_m J_e K P_t) s^3 + (I_m K + I_m I_t J_e K + K K_d P_m P_t) s^2 + \\
 & (I_t K K_d P_m + I_m K K_d P_t) s + I_m I_t K K_d = 0
 \end{aligned}$$

If we render a pure spring with a stiffness value of 40 Nm/rad according to the control gains specified in Table 6.2, numerical analyses indicate that there exists no inertia that destabilizes the system, since passivity is preserved. However, if we set I_t as $0.6 \text{ rad}/(s^2 \text{ Nm})$, we violate passivity. In this case, numerical investigation reveals that the critical inertia value to destabilize the system is equal $5.75 \text{ Nm}/(s^2 \text{ rad})$. In other words, the system can safely interact with inertias which are less than this threshold. However, instability occurs when the environment inertia exceeds this value.

We have experimentally verified these predictions about coupled stability. In particular, we have constructed passivity region plots over two controller gains while keeping the rest of the parameters fixed. These plots resemble to K-B plots of haptic devices [64]. We have chosen 3 passive and 3 non-passive pairs of control gains that are within the vicinity of the passivity boundary to validate the theoretical passivity bounds.

Figure 6.11 presents the $P_t - I_t$ plot of the passivity region. In particular, we fix the P_t gain and select two I_t gains to make the system passive and non-passive, respectively. We observe that all the passive controllers stably interact with the environment such that there exists no inertia value that can destabilize the system. On the other hand, active controllers remain stable only for inertia values up to a certain threshold that depends on the system parameters.

Figure 6.12 presents the $K_d - I_t$ plot of the passivity region. This time, I_t gains are adjusted to obtain passive and non-passive systems for fixed K_d values. This set of experiments also agree with our predictions. Consequently, our experiments serve as a validation of the passivity bounds we have derived in Chapter 4, and the modelling assumptions considered during the derivations.

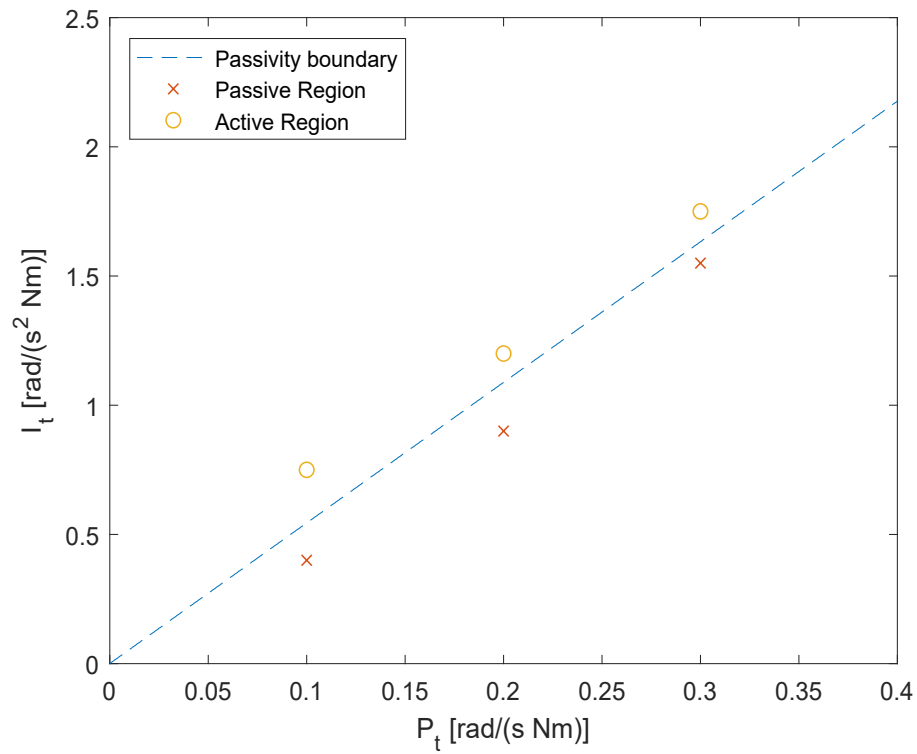


FIGURE 6.11: P_t - I_t plot for experimentally testing coupled stability

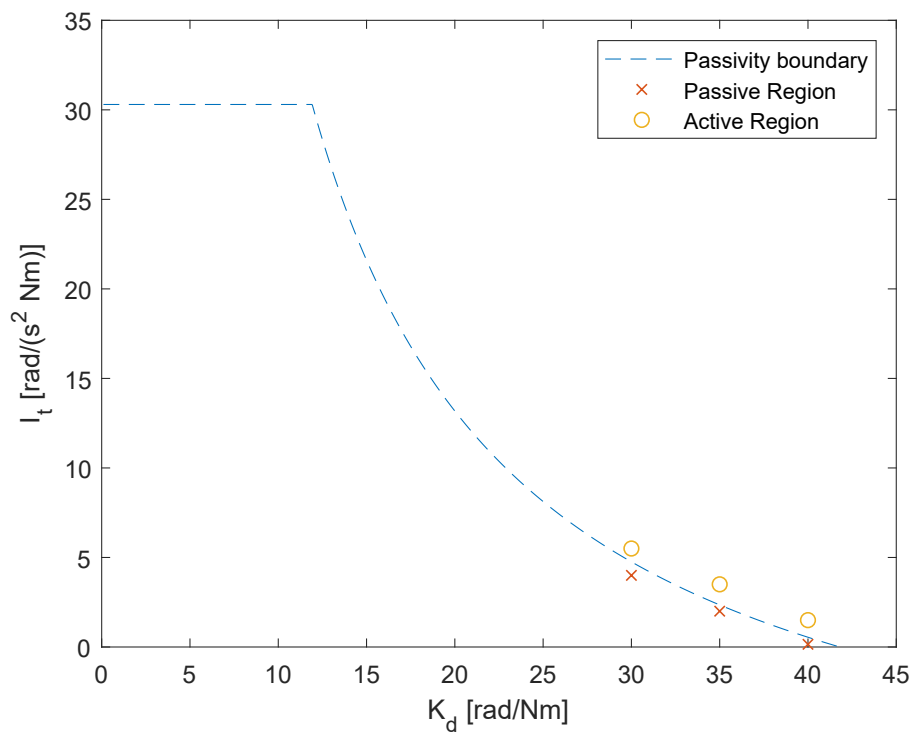


FIGURE 6.12: K_d - I_t plot for experimentally testing coupled stability

Chapter 7

Series Elastic Damping Actuation (SEDA)

This chapter present a useful extension to impedance controlled SEA. We analyze the case where a linear parallel spring-damper is attached as the compliant force-sensing element in SEA. Even though there has been investigations of series damping actuation (SDA) [11] and series elastic damping actuation (SEDA) [34, 39] in the literature, to the best of authors knowledge, SEDA has not been studied with the velocity-force cascaded control architecture.

7.1 Impedance Control of Velocity Sourced Series Elastic Damping Actuation (SEDA)

Figure 7.1 depicts the block diagram of impedance control of velocity sourced SEDA. Here, the complaint force sensing element is a Voigt body (i.e., parallel spring-damper pair) with stiffness K and damping b . Note that the estimated (or measured) torque τ_{EST} does not exactly match with the actual output torque τ_{SEA} . This assumption is due to the practical challenges of estimating the deflection velocity $\Delta\dot{\theta}$, which renders it infeasible for most cases.

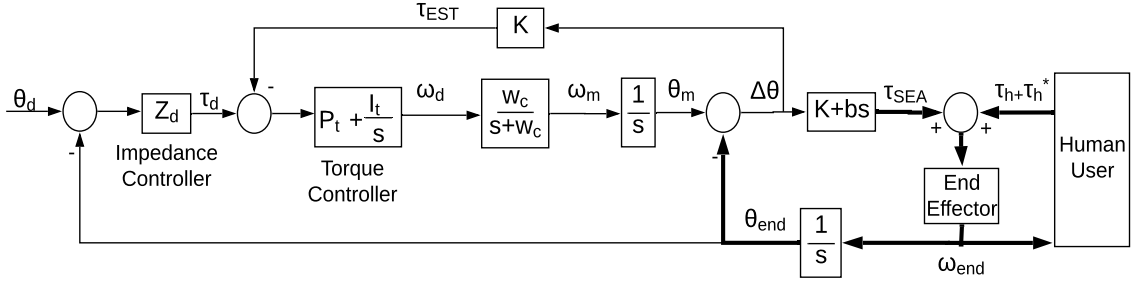


FIGURE 7.1: Velocity-force cascaded control of a series damping elastic actuator

In the previous chapters, we have demonstrated that the interaction with the environment acts as a disturbance to the inner motion loop. However, this can also be aided by feedforward compensation of measured interaction forces. Here, we assume that the interaction forces are eliminated in a feedforward manner and are negligible within the physical bandwidth of the actuator. Consequently, the inner loop is modeled as an ideal first order low pass filter with cut-off frequency w_c . In this case, the output impedance reads as:

$$Z_{out} = \frac{K + bs}{s} \frac{s^3 + w_c s^2 + P_t w_c Z_d s + I_t w_c Z_d}{s^3 + w_c s^2 + P_t w_c K s + I_t w_c K} \quad (7.1)$$

Routh array analysis yields the following necessary and sufficient condition for the stability of the transfer function in Eqn. (7.1):

$$I_t < P_t w_c \quad (7.2)$$

Thereby, Eqn. (7.2) is a *necessary* condition for passivity which imposes an upper bound on the torque integral gain.

Now, let us set the virtual environment as the Voigt model such that $Z_d = K_d + B_d s$. If we analyze the positive-realness as in Chapter 4, we obtain $P(w) = \sum_{n=1}^4 d_{2n} w^{2n}$ where

$$d_8 = b \quad (7.3)$$

$$d_6 = w_c [b w_c + b w_c P_t B_d - K P_t (B_d + b) - b (K_d P_t + B_d I_t)] \quad (7.4)$$

$$d_4 = w_c [(I_t K K_d - I_t K^2) + w_c (K P_t (\alpha b + \beta) - I_t K_d b - \alpha K - I_t \beta b)] \quad (7.5)$$

$$d_2 = w_c^2 I_t^2 K (K_d b + B_d K) \quad (7.6)$$

with $\alpha = B_d I_t + K_d P_t$ and $\beta = K(1 + B_d P_t)$.

The necessary and sufficient conditions to ensure $P(w) \geq 0$ may be derived using Sturm's theorem. However, the polynomial $P(w)$ is quite complex with many parameters which renders it infeasible to obtain an analytical close form solution.

Along these lines, we seek a *sufficient* condition. An obvious solution is to set all coefficients of $P(w)$ positive. Since d_2 and d_8 are already positive, we only need to ensure $d_4 > 0 \wedge d_6 > 0$.

According to this analysis, w_c can assume any positive value without jeopardizing passivity. It also determines the Z-width of the system by introducing limitations on K_d and B_d . I_t is bounded from above by the product $P_t w_c$ due to Eqn. (7.2). Numerical simulations along with the above listed bounds indicate that with the proposed SEDA controller, it is possible to render impedances higher than the impedance of the physical spring-damper. In particular, d_4 and d_6 may be positive even when $K_d > K \vee B_d > b$ so long as w_c is set sufficiently large.

In the following simulations, we use the plant and controller parameters listed in Table 7.1.

TABLE 7.1: Simulation parameters for SEDA rendering Voigt model

Description	Symbol	Value
Stiffness of the complaint element	K	500 Nm/rad
Damping of the complaint element	b	100 Nm.s/rad
Cut-off frequency of the motion loop	w_c	10 Hz
Proportional torque gain	P_t	20 rad/(sNm)
Integral torque gain	I_t	$5 \text{ rad/(s}^2\text{Nm)}$

Figure 7.2 reports the Bode plot when the virtual environment impedance is chosen twice of the physical compliance, such that $K_d = 2K = 1000 \text{ Nm/rad}$ and $B_d = 2b = 200 \text{ Nms/rad}$. Passivity is preserved in this case. This example demonstrates the capability of SEDA to render impedances higher than the impedance of the physical force-sensing element.

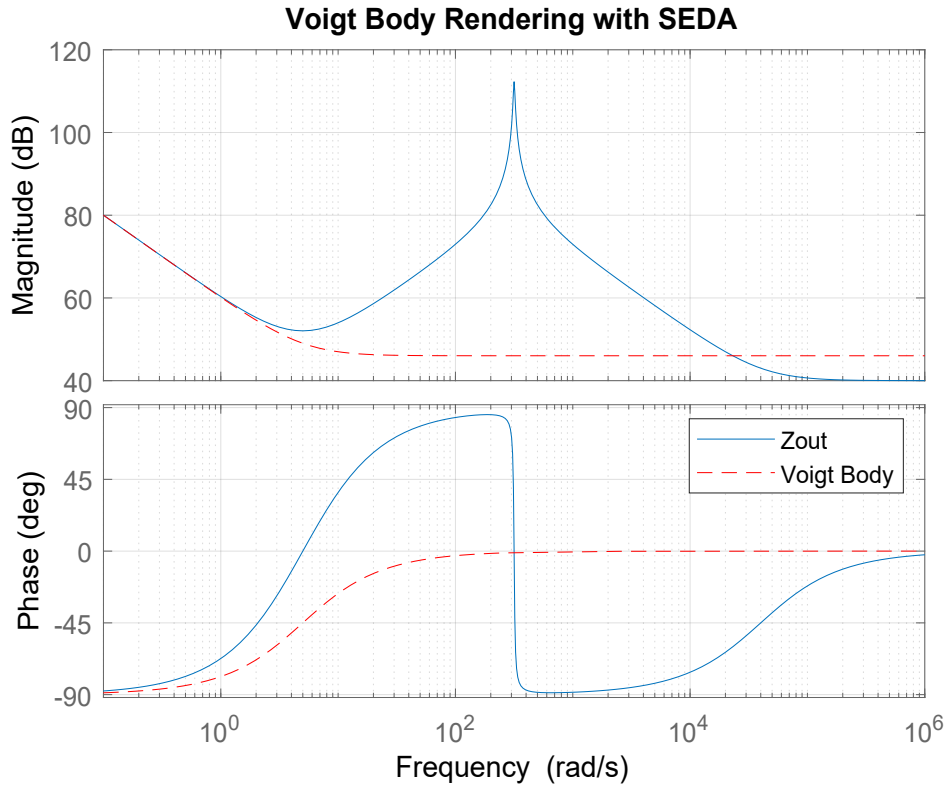


FIGURE 7.2: High impedance rendering with series elastic damping actuator

Figure 7.3 reports the Bode plots when the virtual environment impedance is chosen half of the physical compliance such that $K_d = K/2 = 250 \text{ Nm/rad}$ and $B_d = b/2 = 50 \text{ Nm.s/rad}$. Passivity is preserved in this case, as well.

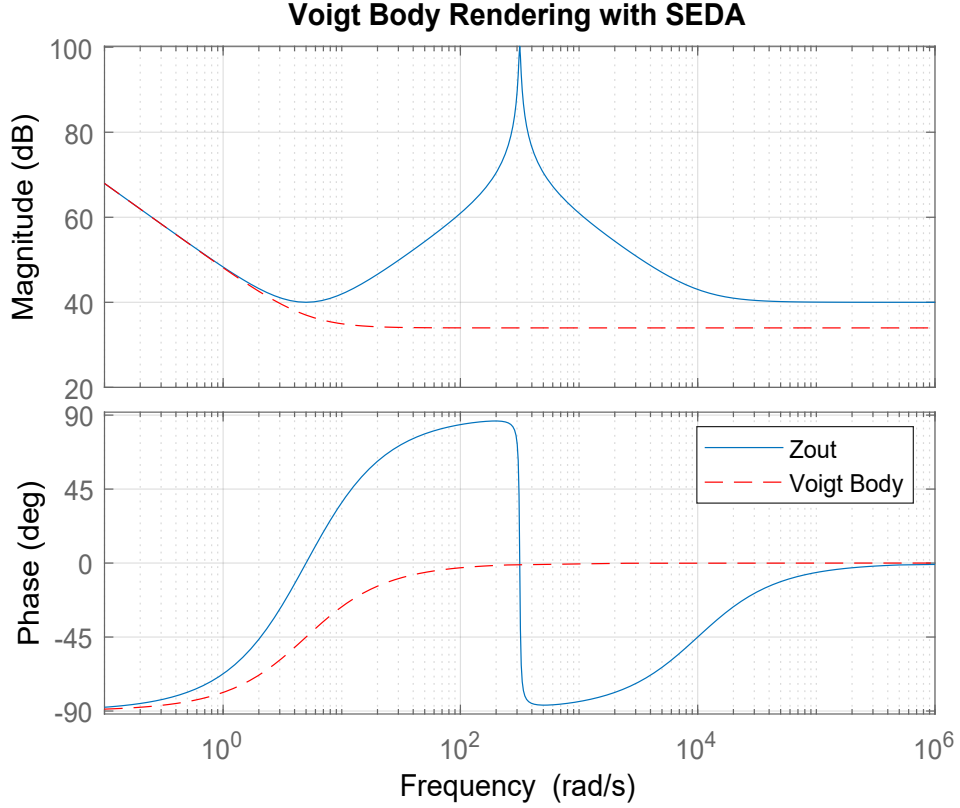


FIGURE 7.3: Low impedance rendering with series elastic damping actuator

7.1.1 Rendering Null Impedance

In this section, we analyze rendering null impedance (i.e., $Z_d = 0$) with velocity-sourced SEDA. Eqn. (7.2) is also a necessary condition for this case. For the passivity analysis, the coefficients of the polynomial $P(w)$ are modified as follows:

$$d_6 = b \quad (7.7)$$

$$d_4 = w_c b (w_c - K P_t) \quad (7.8)$$

$$d_2 = K^2 P_t w_c^2 - I_t K w_c (K + w_c b) \quad (7.9)$$

Similar to the previous case, $d_2 > 0 \wedge d_4 > 0 \wedge d_6 > 0$ is a sufficient condition for passivity. From Eqn. (7.8) we can derive the following lower bound for the cut-off frequency of inner motion loop: $w_c > KP_t$. However, this bound is hard to satisfy as it requires either a very large w_c or very low K and P_t values. Eqn. (7.13) hints at the negative effects of I_t on passivity. Hence, we will set it to zero for the rest of the analyses and simulations in this chapter. Note that, now the lower bound on w_c becomes a *necessary and sufficient* condition for passivity.

Along these lines, we perform a simulation using parameters given in Table 7.1., except for I_t which is set to zero. The system cannot render null impedance passively unless w_c is set unreasonably high, such as $10^4 Hz$, as seen in Figure 7.4.

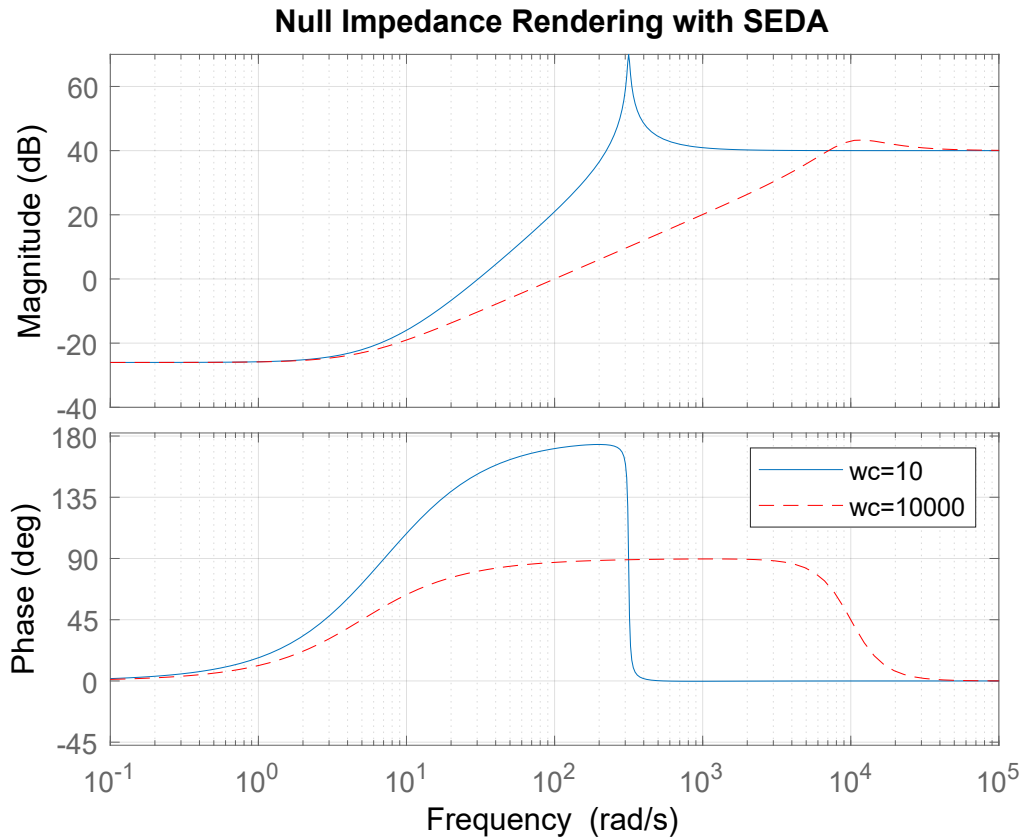


FIGURE 7.4: Null impedance rendering with series elastic damping actuator

7.1.2 Rendering Pure Springs

In this section, we analyze rendering pure springs (i.e., $B_d = 0$) with velocity-sourced SEDA when no integrator is employed in the outer force loop (i.e., $I_t = 0$). Eqn. (7.2) is also a necessary condition for this case. However, the coefficients of the polynomial $P(w)$ are modified as follows:

$$d_6 = b \quad (7.10)$$

$$d_4 = w_c b (w_c - K P_t - K_d P_t) \quad (7.11)$$

$$d_2 = w_c^2 K P_t (K - K_d + K_d P_t b) \quad (7.12)$$

The *sufficiency* bounds do not provide meaningful bound on K_d . However, numerical simulations show that K_d can assume larger values than K , provided that w_c is sufficiently large to preserve passivity. In other words, the introduction of physical damping into SEA makes it possible to passively render virtual springs stiffer than the physical spring so long as the motion control bandwidth of system w_c can be kept sufficiently high.

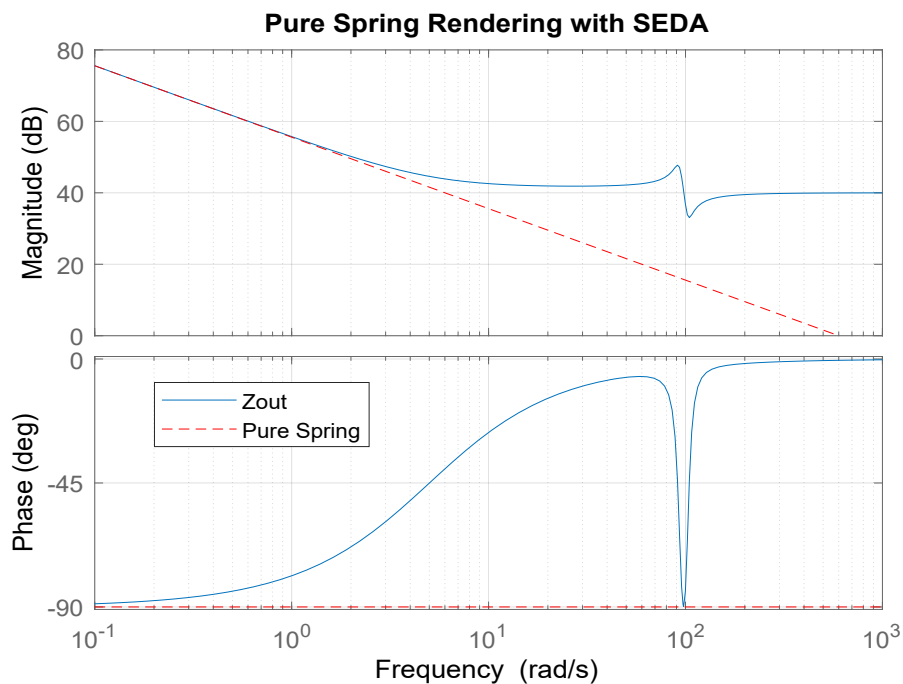


FIGURE 7.5: Stiff wall rendering with series elastic damping actuator

Figure 7.5 presents the Bode plot of the SEDA rendering a pure spring with $530Nm/rad$ stiffness. The control gains and plant parameters are the same as in the case of null impedance. The system is passive since the phase varies between -90° and 0° . The damping of the force sensing element dominates the system at higher frequencies. This example serves as a proof of high stiffness rendering capability of SEDA.

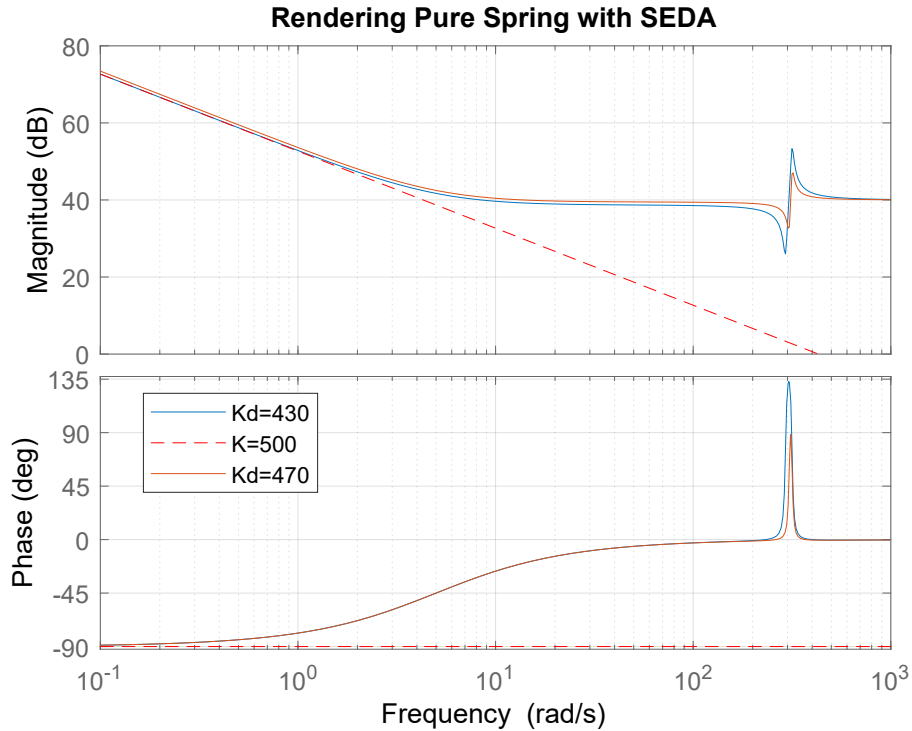


FIGURE 7.6: Pure spring rendering with series elastic damping actuator

Figure 7.6 reports the Bode plot of rendering virtual walls of stiffness values of $470Nm/rad$ and $430Nm/rad$. We observe that the system remains passive for $K_d = 470Nm/rad$, but violates passivity for a relatively softer virtual wall with stiffness of $K_d = 430Nm/rad$. It indicates that SEDA cannot render soft walls passively. Also, we notice that the system quickly deviates from the ideal spring behavior for relatively low frequencies, as can be observed in Figure 7.5 and 7.6. More precisely, the phase of the system is far from -90° at $1 rad/s$. Since humans are capable of easily generating motions at these frequency levels, the operational bandwidth of the system is not acceptable for accurately rendering pure springs.

In particular, it is desirable to stay as close as possible to negative 90 degrees phase up to frequency levels of at least 5 Hz so that the parasitic damping effect is not felt by the user during interactions. Thus, we conclude that since the damping effect dominates the dynamics starting from low frequencies, SEDA does not provide high rendering fidelity for applications that require rendering pure springs.

Chapter 8

Conclusions and Future Work

We have presented the necessary and sufficient conditions to ensure the passivity of cascade-control of SEA for rendering null impedance and pure stiffness models. These conditions extend the sufficiency condition reported in the literature [54, 60, 61] and relaxing these bounds, serve as the least conservative bounds on renderable impedances under the frequency domain passivity paradigm. Our results also prove the necessity of a counter-intuitive second bound on integral gains, that has been neglected in the literature. This bound is crucial as it is imposed due to inevitable physical damping of the actuator; hence, cannot be safely neglected if integral controller is used in both the inner and the intermediate control loops.

While the necessary and sufficient conditions provide the least conservative bounds within the frequency domain passivity paradigm, they may still be conservative. Along these lines, less conservative paradigms, such as time domain passivity [23, 47], complementary stability [5], bounded-impedance absolute stability [22, 65], fractional-order passivity [4, 57] may be utilized to achieve better performance while still ensuring coupled stability of interaction. However, even though they are relatively conservative, frequency domain passivity conditions are valuable as they are

known to provide a fundamental understanding of the underlying trade-offs governing the dynamics of the closed-loop system.

We have experimentally evaluated the effectiveness of velocity sourced SEA and presented detailed design guidelines for haptic rendering of null impedance and pure springs. These two classical linear models serve as the building block of large variety of virtual environments.

We have also studied series elastic damping actuation (SEDA) as an extension to SEA and demonstrated that Voigt body, which is another interesting linear model, can passively be rendered with SEDA. Moreover, SEDA can also passively display environments with even higher impedances than physical impedance of the complaint force-sensing element. On the other hand, its rendering fidelity is low for pure spring and null impedance models. Considering these pros and cons, variable damping SEDA may be a promising scheme that significantly increases the Z-width of SEA haptic devices.

Bibliography

- [1] Online. <http://www.rethinkrobotics.com/products/baxter/>.
- [2] K. Abe, T. Suga, and Y. Fujimoto. Control of a biped robot driven by elastomer-based series elastic actuator. In *IEEE International Workshop on Advanced Motion Control (AMC)*, pages 1–6, 2012.
- [3] Chae H. An and J.M. Hollerbach. Dynamic stability issues in force control of manipulators. In *American Control Conference*, pages 821–827, 1987.
- [4] Y. Aydin, O. Tokatli, V. Patoglu, and C. Basdogan. Stable physical human-robot interaction using fractional order admittance control. *IEEE Transactions on Haptics*, 11(3):464–475, 2018.
- [5] S. P. Buerger and N. Hogan. Complementary stability and loop shaping for improved human–robot interaction. *IEEE Transactions on Robotics*, 23(2):232–244, April 2007.
- [6] S. P. Buerger, H. I. Krebs, and N. Hogan. Characterization and control of a screw-driven robot for neurorehabilitation. In *IEEE International Conference on Control Applications*, pages 388–394, 2001.
- [7] Andrea Calanca, Luca Capisani, and Paolo Fiorini. Robust force control of series elastic actuators. *Actuators*, 3(3):182–204, 2014.
- [8] Andrea Calanca, Riccardo Muradore, and Paolo Fiorini. Impedance control of series elastic actuators: Passivity and acceleration-based control. *Mechatronics*, 47:3748, 2017.

- [9] U. Caliskan, A. Apaydin, A. Otaran, and V. Patoglu. A series elastic brake pedal to preserve conventional pedal feel under regenerative braking. In *IEEE/RSJ International Conference on Intelligent Robots and Systems (IROS)*, pages 1367–1373, 2018.
- [10] U. Caliskan, A. Apaydin, A. Otaran, and V. Patoglu. A series elastic brake pedal to preserve conventional pedal feel under regenerative braking. In *2018 IEEE/RSJ International Conference on Intelligent Robots and Systems (IROS)*, pages 1367–1373, Oct 2018.
- [11] Chee-Meng Chew, Geok-Soon Hong, and Wei Zhou. Series damper actuator: a novel force/torque control actuator. In *4th IEEE/RAS International Conference on Humanoid Robots, 2004.*, volume 2, pages 533–546 Vol. 2, Nov 2004.
- [12] Edward Colgate and Neville Hogan. Robust control of dynamically interacting systems. *International Journal of Control*, pages 65–88, 1988.
- [13] J. E. Colgate and N. Hogan. Robust control of dynamically interacting systems. *International Journal of Control*, 48(1):65–88, 1988.
- [14] J. Edward Colgate and Gerd G. Schenkel. Passivity of a class of sampled-data systems: Application to haptic interfaces. *Journal of Robotic Systems*, 14(1):37–47, 1997.
- [15] James Edward Colgate. *The control of dynamically interacting systems*. PhD thesis, Massachusetts Institute of Technology, 1988.
- [16] I. Diaz, J.J. Gil, and T. Hulin. Stability boundary and transparency for haptic rendering. In Mehrdad Hosseini Zadeh, editor, *Advances in Haptics*, chapter 5, pages 103–125. INTECH, 2010.
- [17] M. Dohring and W. Newman. The passivity of natural admittance control implementations. In *IEEE International Conference on Robotics and Automation*, volume 3, pages 3710–3715, 2003.

- [18] S.D. Eppinger and W.P. Seering. Understanding bandwidth limitations in robot force control. In *IEEE International Conference on Robotics and Automation*, volume 4, pages 904–909, 1987.
- [19] Ahmetcan Erdogan, Besir Celebi, Aykut Cihan Satici, and Volkan Patoglu. AssistOn-Ankle: A reconfigurable ankle exoskeleton with series-elastic actuation. *Autonomous Robots*, pages 1–16, 2016.
- [20] R. B. Gillespie, Dongwon Kim, J. M. Suchoski, Bo Yu, and J. D. Brown. Series elasticity for free free-space motion for free. In *2014 IEEE Haptics Symposium (HAPTICS)*, pages 609–615, Feb 2014.
- [21] P. G. Griffiths, R. B. Gillespie, and J. S. Freudenberg. A fundamental tradeoff between performance and sensitivity within haptic rendering. *IEEE Transactions on Robotics*, 24(3):537–548, June 2008.
- [22] A. Haddadi and K. Hashtrudi-Zaad. Bounded-impedance absolute stability of bilateral teleoperation control systems. *IEEE Transactions on Haptics*, 3(1):15–27, 2010.
- [23] B. Hannaford and Jee-Hwan Ryu. Time-domain passivity control of haptic interfaces. *IEEE Transactions on Robotics and Automation*, 18(1):1–10, Feb 2002.
- [24] Keyvan Hashtrudi-Zaad and Septimiu E. Salcudean. Analysis of control architectures for teleoperation systems with impedance/admittance master and slave manipulators. *The International Journal of Robotics Research*, 20(6):419–445, 2001.
- [25] Simon Haykin. *Active network theory*. Reading, Mass. : Addison-Wesley Pub. Co, 1970.
- [26] Vincent Hayward, Jehangir Choksi, Gonzalo Lanvin, and Christophe Ramstein. Design and multi-objective optimization of a linkage for a haptic interface. *Advances in Robot Kinematics*, 01 1994.
- [27] S. Hirche, A. Bauer, and M. Buss. Transparency of haptic telepresence systems with constant time delay. In *IEEE Conference on Control Applications*, pages 328–333, Aug 2005.

- [28] N. Hogan. Controlling impedance at the man/machine interface. In *International Conference on Robotics and Automation*, volume 3, pages 1626–1631, 1989.
- [29] Neville Hogan. Impedance control: An approach to manipulation: Part i—theory. *Journal of Dynamic Systems, Measurement, and Control*, 107(1):1–7, 1985.
- [30] Russell Duane Howard. *Joint and Actuator Design for Enhanced Stability in Robotic Force Control*. PhD thesis, Massachusetts Institute of Technology, 1990.
- [31] A. Kamadan, G. Kiziltas, and V. Patoglu. Co-design strategies for optimal variable stiffness actuation. *IEEE/ASME Transactions on Mechatronics*, 22(6):2768–2779, 2017.
- [32] Abdullah Kamadan, Gullu Kiziltas, and Volkan Patoglu. A systematic design selection methodology for system-optimal compliant actuation. *Robotica*, pages 1–19, 2018.
- [33] Kerim Deniz Kaya and Levent Cetin. Adaptive state feedback controller design for a rotary series elastic actuator. *Transactions of the Institute of Measurement and Control*, 39(1):61–74, 2017.
- [34] M. J. Kim, A. Werner, F. C. Loeffl, and C. Ott. Enhancing joint torque control of series elastic actuators with physical damping. In *2017 IEEE International Conference on Robotics and Automation (ICRA)*, pages 1227–1234, May 2017.
- [35] Kyoungchul Kong, Joonbum Bae, and M. Tomizuka. A compact rotary series elastic actuator for human assistive systems. *IEEE/ASME Transactions on Mechatronics*, 17(2):288–297, April 2012.
- [36] D. A. Lawrence. Stability and transparency in bilateral teleoperation. *IEEE Transactions on Robotics and Automation*, 9(5):624–637, Oct 1993.
- [37] H. Munawar and V. Patoglu. Gravity-Assist: A series elastic body weight support system with inertia compensation. In *IEEE/RSJ International Conference on Intelligent Robots and Systems (IROS)*, pages 3036–3041, 2016.

- [38] Wyatt Newman. Stability and performance limits of interaction controllers. *ASME Transactions of The Journal of Dynamic Systems Measurement and Control*, 114, 12 1992.
- [39] Jakob Oblak and Zlatko Matjacic. Design of a series visco-elastic actuator for multi-purpose rehabilitation haptic device. In *Journal of NeuroEngineering and Rehabilitation*, 2010.
- [40] Katsuhiko Ogata. *Modern Control Engineering*. Pearson, 5 edition, 2009.
- [41] Sehoon Oh and Kyoungchul Kong. High-precision robust force control of a series elastic actuator. *IEEE/ASME Transactions on Mechatronics*, 22(1):71–80, 2016.
- [42] Ata Otaran, Ozan Tokatli, and Volkan Patoglu. Hands-on learning with a series elastic educational robot. In *Proceedings of the EuroHaptics (EuroHaptics 2016) as Lecture Notes in Computer Science*, 2016.
- [43] N. Paine, Sehoon Oh, and L. Sentis. Design and control considerations for high-performance series elastic actuators. *IEEE/ASME Transactions on Mechatronics*, 19(3):1080–1091, 2014.
- [44] G.A. Pratt and M.M. Williamson. Series elastic actuators. In *IEEE/RSJ International Conference on Intelligent Robots and Systems*, volume 1, pages 399–406, 1995.
- [45] G.A. Pratt, P. Willisson, C. Bolton, and A. Hofman. Late motor processing in low-impedance robots: impedance control of series-elastic actuators. *American Control Conference*, pages 3245–3251, 2004.
- [46] D.W. Robinson, J.E. Pratt, D.J. Paluska, and G.A. Pratt. Series elastic actuator development for a biomimetic walking robot. In *IEEE/ASME International Conference on Advanced Intelligent Mechatronics*, pages 561–568, 1999.
- [47] Jee-Hwan Ryu, Dong-Soo Kwon, and B. Hannaford. Stability guaranteed control: time domain passivity approach. *IEEE Transactions on Control Systems Technology*, 12(6):860–868, Nov 2004.

- [48] Mine Sarac, Mehmet Alper Ergin, Ahmetcan Erdogan, and Volkan Patoglu. AssistOn-Mobile: A series elastic holonomic mobile platform for upper extremity rehabilitation. *Robotica*, 32:1433–1459, 12 2014.
- [49] T. Schau and A. Peer. Parameter-space transparency analysis of teleoperation systems. In *IEEE Haptics Symposium*, pages 111–116, March 2012.
- [50] J. W. Sensinger and R. F. f. Weir. Improvements to series elastic actuators. In *IEEE/ASME International Conference on Mechatronics and Embedded Systems and Applications*, 2006.
- [51] J. W. Sensinger and R. F. f. Weir. Unconstrained impedance control using a compact series elastic actuator. In *IEEE/ASME International Conference on Mechatronics and Embedded Systems and Applications*, 2006.
- [52] Yusuf Mert Senturk and Volkan Patoglu. MRI-VisAct: A bowden cable-driven mri compatible series viscoelastic actuator. *Transactions of the Institute of Measurement and Control, Sage*, 40(8):2440–2453, 2018.
- [53] Fabrizio Sergi and Marcia K. OMalley. On the stability and accuracy of high stiffness rendering in non-backdrivable actuators through series elasticity. *Mechatronics*, 26:64 – 75, 2015.
- [54] N. L. Tagliamonte and D. Accoto. Passivity constraints for the impedance control of series elastic actuators. *Journal of Systems and Control Engineering*, 228(3):138–153, 2014.
- [55] M. Tavakoli, A. Aziminejad, R. V. Patel, and M. Moallem. Enhanced transparency in haptics-based master-slave systems. In *American Control Conference*, pages 1455–1460, July 2007.
- [56] O. Tokatli and V. Patoglu. Optimal design of a micro series elastic actuator. In *International Design Engineering Technical Conferences and Computers and Information in Engineering Conference*, 2010.

- [57] O. Tokatli and V. Patoglu. Stability of haptic systems with fractional order controllers. In *IEEE/RSJ International Conference on Intelligent Robots and Systems*, pages 1172–1177, Sept 2015.
- [58] E. Treadway, Y. Yang, and R. B. Gillespie. Decomposing the performance of admittance and series elastic haptic rendering architectures. In *2017 IEEE World Haptics Conference (WHC)*, pages 346–351, June 2017.
- [59] R. Unal, G. Kiziltas, and V. Patoglu. A multi-criteria design optimization framework for haptic interfaces. In *Symposium on Haptic Interfaces for Virtual Environment and Teleoperator Systems*, pages 231–238, 2008.
- [60] H. Vallery, R. Ekkelenkamp, H. van der Kooij, and M. Buss. Passive and accurate torque control of series elastic actuators. In *IEEE/RSJ International Conference on Intelligent Robots and Systems*, pages 3534–3538, 2007.
- [61] Heike Vallery, Jan Veneman, and Edwin van Asseldonk. Compliant actuation of rehabilitation robots. *IEEE Robotics & Automation Magazine*, 15(3):60–69, 2008.
- [62] J. F. Veneman, R. Ekkelenkamp, R. Kruidhof, F. C. T. van der Helm, and H. van der Kooij. A series elastic- and bowden-cable-based actuation system for use as torque actuator in exoskeleton-type robots. *The International Journal of Robotics Research*, 25(3):261–281, 2006.
- [63] Meng Wang, Lei Sun, Wei Yin, Shuai Dong, and Jingtai Liu. A novel sliding mode control for series elastic actuator torque tracking with an extended disturbance observer. *IEEE International Conference on Robotics and Biomimetics*, pages 2407–2412, Jun 2015.
- [64] D. W. Weir and J. E. Colgate. Stability of haptic displays. *Haptic Rendering: Foundations, Algorithms and Applications*, pages 123–156, 2008.
- [65] B. Willaert, M. Franken, H. Van Brussel, and E. B. Vander Poorten. On the use of shunt impedances versus bounded environment passivity for teleoperation systems. In *IEEE International Conference on Robotics and Automation*, pages 2111–2117, 2011.

- [66] Hanseung Woo, Byeonghun Na, and Kyouchul Kong. Design of a compact rotary series elastic actuator for improved actuation transparency and mechanical safety. *IEEE International Conference on Robotics and Automation*, 2017.
- [67] Gordon Wyeth. Demonstrating the safety and performance of a velocity sourced series elastic actuator. In *IEEE International Conference on Robotics and Automation*, pages 3642–3647, 2008.
- [68] Michael Zinn, Oussama Khatib, Bernard Roth, and J. Kenneth Salisbury. Large workspace haptic devices - a new actuation approach. *Symposium on Haptic Interfaces for Virtual Environment and Teleoperator Systems*, 2008.